MET O 11 TECHNICAL NOTE NO 172

An Investigation of an Instability in the Operational Data Assimilation scheme associated with High Topography

by

T B Fugard and W H Lyne

Met O 11 (Forecasting Research Branch)
Meteorological Office
London Road
Bracknell
Berks

April 1983

JB

MET O 11 TECHNICAL NOTE NO 172

An Investigation of an Instability in the Operational Data Assimilation Scheme associated with High Topography

by T B Fugard and W H Lyne

Summary

During the operational trials of Summer 1982, a recurring feature of the analysis was a tendency to instability to the west of the Peruvian Andes. A particularly bad case, for 12Z, 28/6/82, is examined in depth. It is found that the instability is caused by the data from a single coastal station and is associated with the selection and analysis of data on pressure levels. An experiment in which selection and optimal interpolation analysis weights are calculated using σ instead of p gives a marked improvement. The use of sigma level analysis is also successful in removing an instability in a second case.

1. Introduction

This note presents the results of a study into a recurring problem in the operational data assimilation scheme (see Lyne et al 1983 for a description of the scheme). This manifests itself as an instability near the edge of high topography in such regions as the Andes, Greenland and the Himalayas. A particularly severe case occurred to the west of the Andes in the analysis for 12Z on 28 June 1982. Figure 1a-f show the wind and temperature fields for standard levels from 850-150 mb. An instability in the wind field is evident throughout a large depth of the atmosphere in the region 20-30S, 65-80W, and a corresponding 'dipole' (closely adjacent low/high regions) in the temperature field is strongest at 850 mb, 700 mb and above 200 mb.

The six hour forecast valid at the analysis time does not show the instability (Fig 2a and b), although the wind field in the area of interest is rough. Fig 3a and b show the 700 mb and 300 mb wind and temperature fields of a 24 hour forecast from the 12Z analysis. It is seen that the instability in the analysis has largely been dissipated by the model and the effects on the circumpolar jet are probably small in this case. In other synoptic situations, however, such an instability in the analysis may have serious consequences in a subsequent forecast.

It should be pointed out that the version of the assimilation model that was in use in June 1982 differs slightly from the current version in that damping of vertically integrated divergence was used instead of level by level divergence damping (Dumelow, 1983). Further, the relaxation coefficient (see § 2) for the assimilation was constant for all variables at 0.1 whereas in the current version it varies linearly in time from 0 to 0.125.

The experiments reported in this note fall naturally into two classes. The first concerns preliminary runs to isolate the 12Z data responsible for the instability. The second concerns changes in the formulation of the scheme

including the effect of divergence damping; a change in the formulation of horizontal diffusion; the use of the current operational scheme, and finally a change in the data selection and optimal interpolation step.

2. A Brief Description of the Assimilation Scheme

The details of the current operational scheme are given in Lyne et al (1983). The version of the assimilation model in use on 28/6/82 is described in Fugard and Lyne (1983) and the two versions of divergence damping (vertically integrated and level by level) are considered in detail in Dumelow (1983). In the following paragraphs aspects of the scheme pertinent to this study are given.

2.1 Data Selection

For a grid point g, the nearest 20 observations are chosen with horizontal distance less than 5.25 degrees of latitude from g. From each of these observations, relevant data at a pressure level p_i for which $|\ln(p_i/p_g)|$ is a minimum is chosen (so long as $|\ln(p_i/p_g)| < 1.5$), and finally at most seven of these are selected according to their importance in reducing the expected analysis error of optimal interpolation.

One of the experiments changes this selection so that $|\ln(\sigma_i/\sigma_g)|$ replaces $|\ln(p_i/p_g)|$, where σ_i and σ_g are observation and grid point sigma levels; (here $\sigma_i = p_i / p_*$ where p_* is the background field surface pressure at the observation point). This shall be referred to as sigma selection as distinct from pressure selection.

2.2 Statistical Interpolation (OI)

Let g be updated by N observations and let ε^b_g, ε^b_i be the prediction (background) errors at grid point g and observation point i, and let ε^o_i be the observation error at i. The weights W_{ig}, $i=1,\ldots,N$ are given by the solution of the linear equations, $j = 1,\ldots,N$,

$$\sum_{i=1}^{N} (\overline{\varepsilon_i^b \varepsilon_j^b} + \overline{\varepsilon_i^o \varepsilon_j^o}) W_{ig} = \overline{\varepsilon_j^b \varepsilon_g^b}, \quad (1)$$

where $\overline{(\quad)}$ represents ensemble average. The prediction covariance is modelled by

$$\overline{\varepsilon_i^b \varepsilon_j^b} = \overline{\varepsilon_i^{b\,2}}^{1/2} \mu_{ij} \overline{\varepsilon_j^{b\,2}}^{1/2},$$

where the correlation for geopotential height is given by

$$\mu_{ij} = \exp\left[-a r_{ij}^2 - b \ln^2 (p_i / p_j)\right]. \quad (2)$$

Here a and b are constants, r_{ij} is the horizontal distance between i and j and p_i, p_j are pressure levels. From this, the covariances for potential temperature, surface pressure and wind components are derived using the hydrostatic and geostrophic relations (see Lyne et al 1983 for details). Multivariate covariances can also be derived but at present the analysis is univariate.

In one of the experiments (2) is replaced by

$$\mu_{ij} = \exp\left[-a r_{ij}^2 - b \ln^2 (\sigma_i / \sigma_j)\right]. \quad (3)$$

A rigorous derivation of correlations of wind etc introduces cross-correlations between the variables, a detail that is not justified in the present scheme. The important property of μ_{ij} is to give horizontal correlation functions which behave like those in Fig 1 of Bergman (1979). In view of this, the correlations of wind, potential temperature, surface pressure and humidity mixing ratio are taken to be as they were for pressure level analysis but with p replaced by the corresponding σ. For example (3) replaces (2).

2.3 Dynamic Assimilation

Let ψ be a model variable. Data is assimilated at grid point g via the equations

$$\psi_g^*(t+1) = F(\psi(t))$$

$$\psi_g(t+1) = \psi_g^*(t+1) + \lambda \sum_{i=1}^{N} W_{ig} (\psi_i^o - \psi_i(t)) \quad (4)$$

where W_{ig} are from (1), F is the action of the forecast model (including 'physics') through one timestep, $\psi_i(t)$ is the model field at the observation point i, λ is the relaxation coefficient and t is the timestep. It is important to note that $\psi_i(t)$ is obtained from the ψ field by bilinear interpolation ALONG SIGMA SURFACES followed by linear interpolation in the vertical in ln p.

Foreman (1981) has considered non-linear horizontal diffusion in a sigma coordinate model and recommends diffusion on σ-surfaces near to the earth's surface and on P-surfaces above σ-level 5 (σ= 0.79). This has been implemented and one of the experiments carried out on this case was to apply diffusion on σ-surfaces throughout the atmosphere to eliminate the discontinuity in formulation that occurs near to the level with the largest instability in Fig 1.

3. Preliminary Experiments

3.1 Data Studies

Some experiments were carried out to isolate the 12Z data responsible for the instability in Fig 1. It was found that the wind data from the ascent at station 85442 (23.45, 70.4W) caused the problem. Table 1 shows the wind observation as presented to the analysis and the vector wind difference from the 6 hour forecast valid at 12Z.

Table 1 Wind observation for 12Z, 28/6/82 at 85442 (23.45, 70.4W)

Pressure Level (mb)	Vector Wind (°, KT)	Vector Difference from 6 HR forecast (°, KT)
884.3	(190, 4)	(165, 18.3)
881.2	(112. 2.3)	(154, 18.7)
862.1	(97, 2.7)	(156, 31.7)
826.7	(74, 3.5)	(150, 29.3)
769.1	(51, 5.7)	(153, 24.4)
698.5	(40, 8.8)	(346, 23.3)
610.3	(220, 3.2)	(146, 4.1)
521.9	(229, 17.2)	(8.5, 17.2)

The effect was strong when winds above 690 mb were omitted and weak when winds below 690 mb of this ascent were omitted. If only winds up to 700 mb were included, the instability was weak, implicating the level 698.5 mb wind. However, an assimilation of only this level of wind data from the observation produced no instability. It appears that all the wind data below the general level of the model Andes topography is important for the effect.

It should be pointed out that the model height at station 85442 is higher than the real height due to smoothing of topography. This leads to difficulties in the extraction of the data at the pressures of the model sigma levels. However, any assimilation scheme ought to be able to cope with an observation like that in Table 1.

3.2 Studies in the Assimilation Model Formulation

The experiments reported in this section and in § 3.3 were carried out using only the wind data of 85442.

a. Dey (1978) reports that difficulties near to topography were found in using a form of divergence damping. The damping in the model was removed with little impact on the instability.

b. Horizontal diffusion was carried out on σ-surfaces at all levels and again the instability appeared.

c. The relaxation coefficient λ in (4) was reduced from 0.1 to as low as 0.03. The instability continued to appear but was weaker. It should be noted that a relaxation coefficient of 0.03 was tried for some weeks in the operational scheme but it had an adverse effect on the analysis of jet streams.

3.3 Study of the Effect of the Current Assimilation Model

Experiments reported in Fugard and Lyne (1983) and Dumelow (1983) indicate that it is beneficial to vary the relaxation coefficient linearly in

time and that damping of divergence should be carried out at each model level instead of on the integrated column divergence. The effect of these on the instability was examined.

a. The relaxation coefficient λ was varied linearly in time from 0 to 0.1 through the 6 hour assimilation. This reduced the effect of the instability, as can be seen from Fig 4a-c (timestep by timestep values of regional rms pressure tendency, divergence and sigma dot) and Fig 5b (the analysis wind at $\sigma = 0.69$).

b. The current operational assimilation model was used (with final value of λ set at 0.125). This showed a slightly less dramatic instability than that in a. (see Figs 4a. and 5c).

It can be seen that, although the tendency to instability is reduced in a. and b., it is still present.

4. A Possible Mechanism for the Instability

In this section it is argued that the instability is the result of a positive feedback process initiated by the use of inappropriate data to update certain grid points.

Firstly, it should be pointed out that certain data may be appropriate for some analysis schemes but not for others. For example, in a scheme that interpolates fields (rather than increments), a ship wind observation may be inappropriate for updating the free atmosphere; whereas in a scheme where increments from a model background field are analysed, the observation may be useful if the model field has a realistic boundary layer wind profile. Similarly, a static OI analysis on pressure surfaces may be suitable for providing initial conditions for a sigma coordinate model, but pressure selection and analysis may be inappropriate for data on the edge of topography for dynamic assimilation via equations (4) using a sigma co-ordinate model.

Figure 6 shows the current situation for updating grid point g at 800 mb where σ is, say, 0.8 - a free atmosphere point. The observation has, say, $P_* = 820$ mb, so the data selected will be the lower boundary layer observation at i. At each timestep, the observation at i will be compared with the model values at h and k via interpolation and equations (4). These may behave significantly differently from the model at g. This effect is spread through a large depth of the lower troposphere and may eventually give rise to large imbalances in the sensitive pressure gradient term of the equations of motion (via advection of large errors onto the observation point) which has the form

$$-\frac{1}{a\cos\Theta}\left(\frac{\partial\Phi}{\partial\psi}+c_p\sigma^k\Theta\frac{\partial\Pi_*}{\partial\psi}\right),\quad -\frac{1}{a}\left(\frac{\partial\Phi}{\partial\Theta}+c_p\sigma^k\Theta\frac{\partial\Pi_*}{\partial\Theta}\right), \quad (5)$$

where a is the radius of the earth, Θ is latitude, ψ is longitude, Φ is geopotential, Π_* is $(P_*/1000)^k$ and Θ is potential temperature.

Figure 7 shows the situation where σ is used as the basis for data selection. Now the value at g more directly influences the increments calculated in (4). It appears reasonable that the selection and analysis should be such that the data chosen is at a position where the i-g prediction error correlation is maximum. Hence changing the correlation function (2) to (3) is natural with sigma level selection. This shall be referred to as sigma level analysis as distinct from the current pressure level analysis.

5. Experiments with Sigma Level Analysis

The 12Z, 28/6/82 analysis was rerun using the sigma level analysis and the version of the assimilation model with damping of integrated divergence and relaxation coefficient constant at 0.1. It can be seen from the timestep by timestep rms pressure tendency, divergence and sigma dot in the region (Fig 4 a-c experiment iv.) that there is no tendency for instability and the winds at $\sigma = 0.69$ in Figure 5d are of reasonable magnitude, if somewhat incoherent in direction. Figure 8a and b show the 700 mb and 500 mb wind fields from the sigma level analysis and should be compared with Fig 1b and c.

In Fugard and Lyne (1983) it was noted that instabilities near to topography could be initiated by using a large value of the relaxation coefficient λ in equation (4). Figure 9a and b show the Asian/N Pacific 700 mb and 500 mb wind field for a pressure level analysis and relaxation coefficient $\lambda = 0.3$ in the assimilation. The data time is 12Z on 4/11/82. Instabilities are evident near 25N 95E and 38N 80E. Figure 10a and b show the corresponding charts for a sigma level analysis with $\lambda = 0.3$ in the assimilation. It can be seen that the instability is not present.

Table 2 shows the verification figures against observations for the two analyses with $\lambda = 0.3$. The removal of the instability by the sigma level analysis is evident in the wind verification figures for the mid troposphere. The slight increase in error for high level winds may indicate the unsuitability of sigma level analysis for analysing jet streams.

6. Conclusions

This study has examined an instability near to topography. It is concluded that selecting data and analysing on pressure surfaces is inappropriate for the lower troposphere near mountains and that analysing on sigma surfaces effects an improvement. It could be argued that one possible cure for the problem would be to carry out horizontal interpolation to produce $\sqrt{T_i}(t)$ in (4) on pressure surfaces. This would, however, require significant vertical extrapolation below topography.

It appears that the best solution would be to select data and analyse with respect to a hybrid vertical coordinate which approximates sigma near to the surface and pressure at the jet stream levels. Such a coordinate has been used for forecast models; see, for example Simmons and Burridge 1982.

Table 2 RMS errors of analyses against included observations. Relaxation coefficient $\lambda = 0.3$

Key N = Latitude 30N-90N

T = Latitude 30N-30S

S = Latitude 30S-90S

L = Pressure band $P > 700$ mb

M = Pressure band $400 < P \leq 700$ mb

H = Pressure band $P \leq 400$ mb

P_* = Surface pressure

Ⓗ = Potential temperature

U = Vector wind

Variable and Region	RMS errors, P level analysis	RMS errors, σ-level analysis
P_*, N (mb)	1.90	1.89
P_*, T (mb)	1.56	1.46
P_*, S (mb)	1.40	1.48
Ⓗ, NL (^oK)	1.03	0.98
Ⓗ, TL (^oK)	2.25	2.24
Ⓗ, SL (^oK)	1.26	1.32
Ⓗ, NM (^oK)	1.11	0.94
Ⓗ, TM (^oK)	1.43	1.37
Ⓗ, SM (^oK)	2.89	2.76
Ⓗ, NH (^oK)	2.10	2.23
Ⓗ, TH (^oK)	2.44	2.48
Ⓗ, SH (^oK)	2.58	2.57
U , NL (KT)	4.73	4.28
U , TL (KT)	4.73	4.25
U , SL (KT)	5.90	4.12
U , NM (KT)	7.83	4.13
U, TM (KT)	13.61	2.39
U, SM (KT)	3.33	3.36
U, NH (KT)	8.01	7.96
U, TH (KT)	6.08	6.26
U, SH (KT)	7.62	8.33

References

Bergman, K.H. 1979 'Multivariate analysis of temperatures and winds using optimum interpolation'. Mon. Wea. Rev. 107, 1423-1444.

Dey, C.H. 1978 'Noise suppression in a primitive equation model'. Mon. Wea. Rev. 106, 159-173.

Dumelow, R.K. 1983 'Some experiments in the use of divergence damping in the operational assimilation model'. Met O 11 Technical Note No 171.

Foreman, S.J. 1981 'On the calculation of the horizontal diffusion terms in a sigma-coordinate model'. Met O 11 Working Paper No 24.

Fugard, T.B. and Lyne, W.H. 1983 'Preliminary experiments with the new operational data assimilation scheme'. Met O 11 Technical Note No 169.

Lyne W.H., Little, C.T., Dumelow, R.K., Bell, R.S. 1983 'The operational data assimilation scheme' Met O 11 Technical Note No 168.

Simmons, A.J. and Burridge, D.M. 1982 'An energy and angular momentum conserving finite-difference scheme and hybrid vertical coordinates'. Mon. Wea. Rev. 109, 758-766.

Legend of Figures

Figure 1a-f — Standard level wind and temperature charts for the analysis for 12Z, 28/6/82.

Figure 2a and b — 500 mb and 300 mb wind charts from a 6 hour forecast valid at 12Z, 28/6/82.

Figure 3a and b — 700 mb and 300 mb wind and temperature charts from a 24 hour forecast from the analysis for 12Z, 28/6/82.

Figure 4 — RMS diagnostics for area 13.5-28.5S, 99.4-52.5W against time during assimilation.

a. surface pressure tendency

b. divergence

c. sigma dot

Figure 5 — Grid point winds for σ-level 6 (σ= 0.69), rows 75-78 and points 152-155 for analyses.

a. Relaxation coefficient 0.1, pressure level analysis, damping of vertically integrated divergence.

b. Relaxation coefficient varying linearly 0→0.1, pressure level analysis, damping of vertically integrated divergence.

c. Relaxation coefficient varying linearly 0→0.125, pressure level analysis, damping divergences level by level.

d. Relaxation coefficient 0.1, sigma level analysis, damping of vertically integrated divergence.

Figure 6 — Schematic diagram of pressure level selection.

Figure 7	Schematic diagram of sigma level selection.
Figure 8a and b	700 mb and 500 mb wind charts for sigma level analysis for 12Z, 28/6/82, relaxation coefficient 0.1.
Figure 9a and b	700 mb and 500 mb wind charts for pressure level analysis for 12Z, 4/11/82, relaxation coefficient 0.3.
Figure 10a and b	700 mb and 500 mb wind charts for sigma level analysis for 12Z, 4/11/82, relaxation coefficient 0.3.

DT 12Z 28/6/82 VT 12Z 28/6/82 MAIN T+0 DDFF KT. STR 850 MB

DT 12Z 28/6/82 VT 12Z 28/6/82 MAIN T+0 TEMPERATURE C. 850 MB

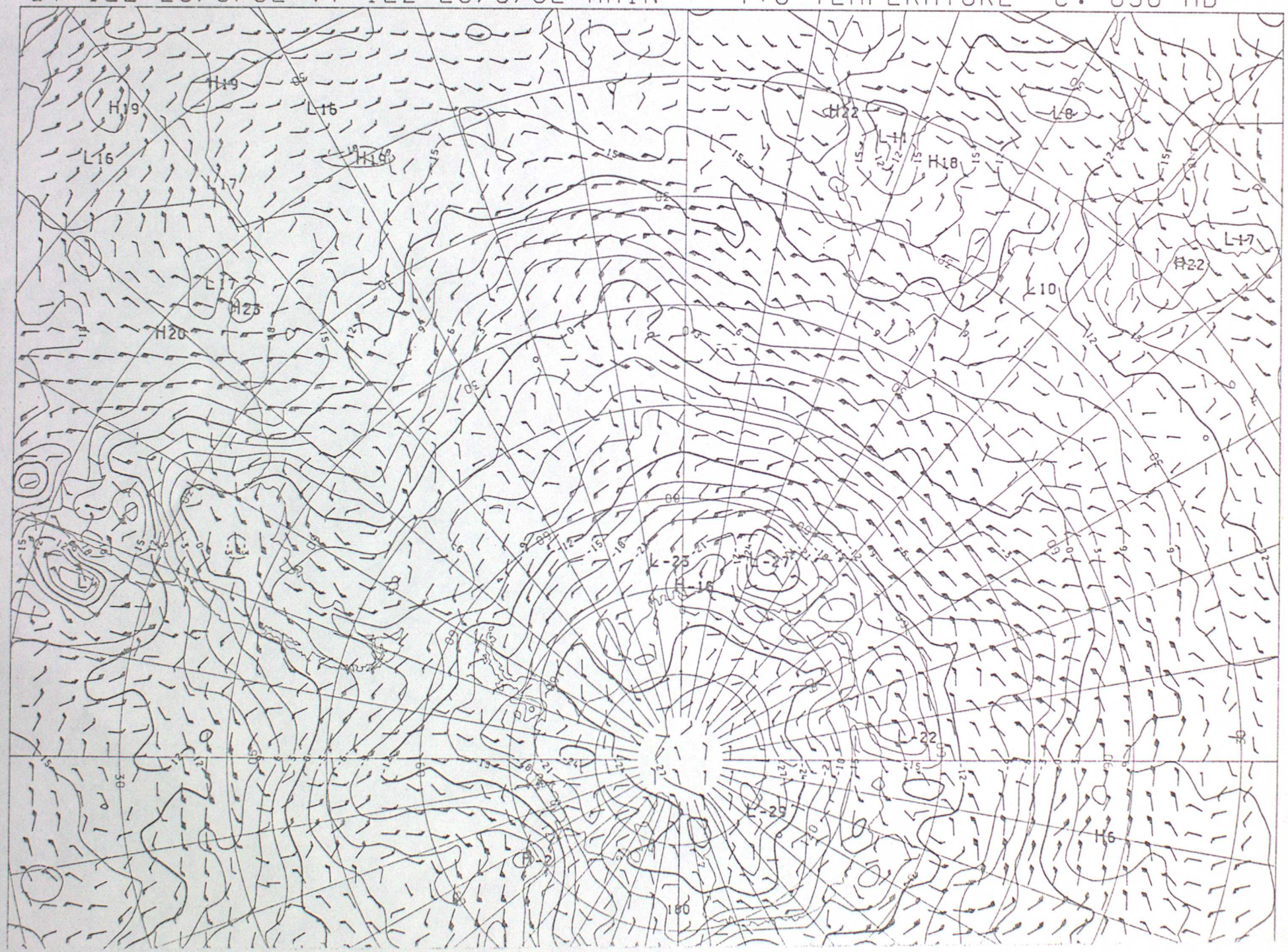

FIG 1(a)

DT 12Z 28/6/82 VT 12Z 28/6/82 MAIN T+0 DDFF KT. STR 700 MB

DT 12Z 28/6/82 VT 12Z 28/6/82 MAIN T+0 TEMPERATURE C. 700 MB

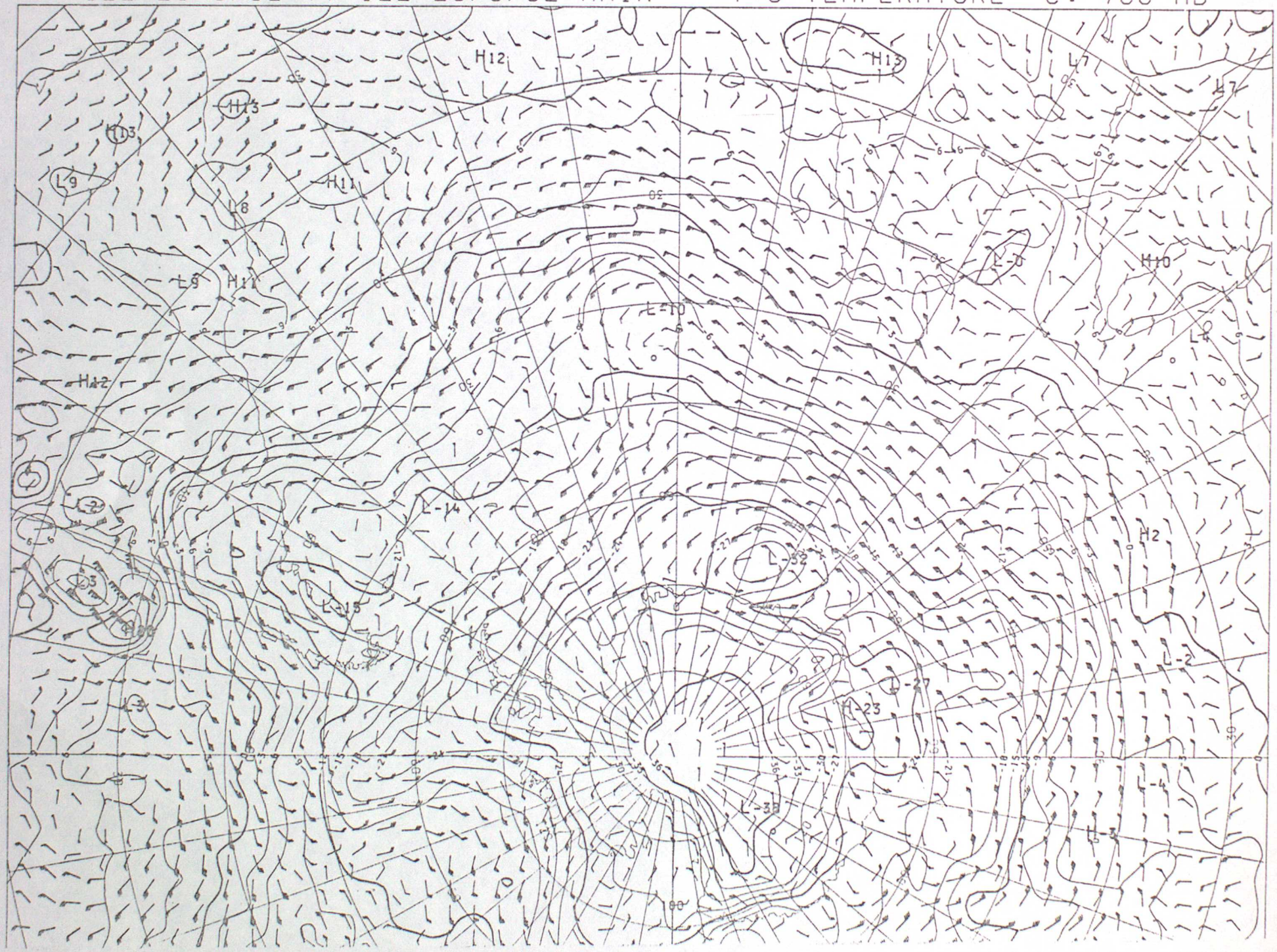

FIG 16)

DT 12Z 28/6/82 VT 12Z 28/6/82 MAIN T+0 DDFF KT. STR 500 MB

DT 12Z 28/6/82 VT 12Z 28/6/82 MAIN T+0 TEMPERATURE C. 500 MB

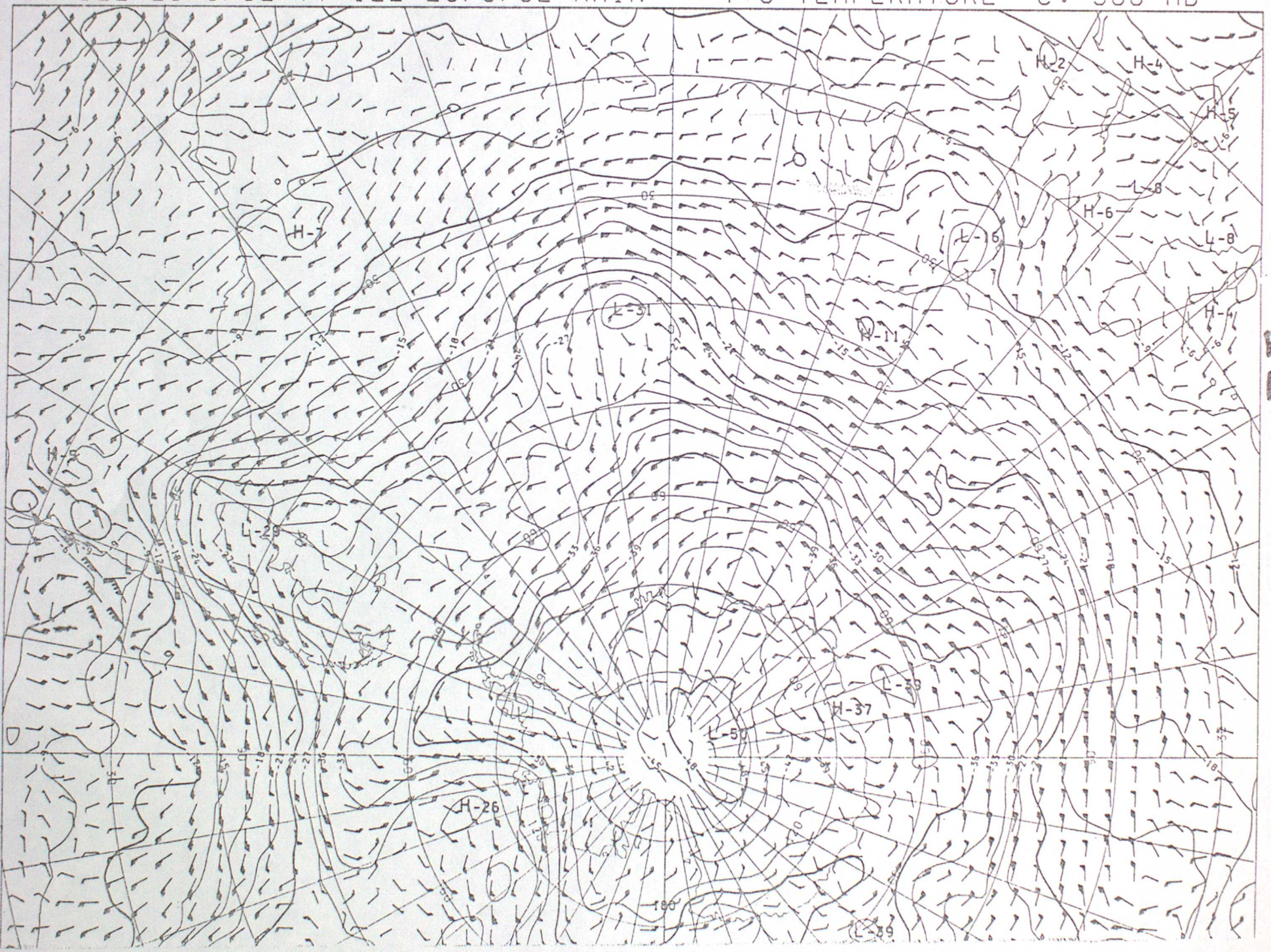

FIG 1(c)

DT 12Z 28/6/82 VT 12Z 28/6/82 MAIN T+0 DDFF KT. STR 300 MB

DT 12Z 28/6/82 VT 12Z 28/6/82 MAIN T+0 TEMPERATURE C. 300 MB

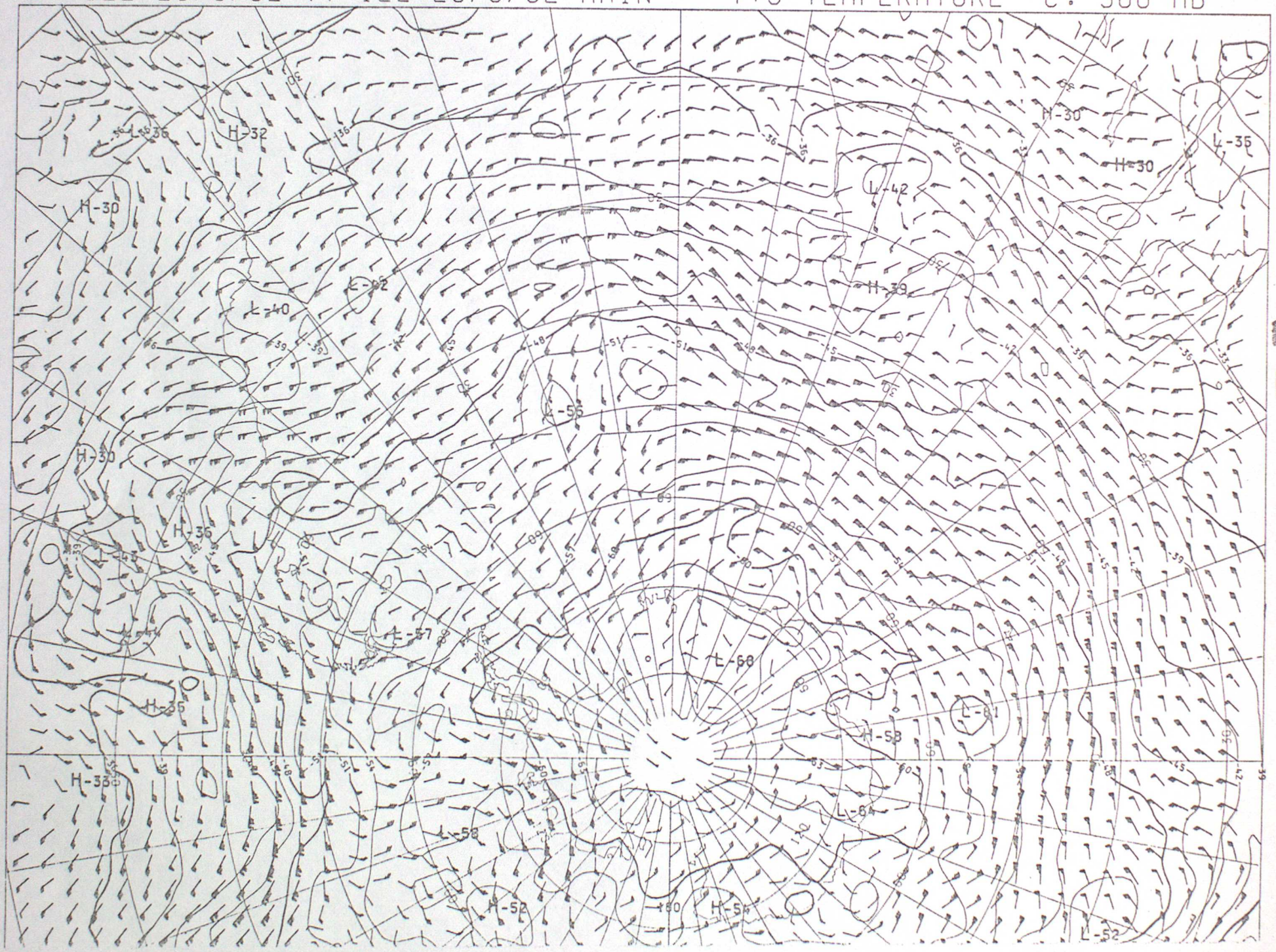

FIG 1(d)

DT 12Z 28/6/82 VT 12Z 28/6/82 MAIN T+0 DDFF KT. STR 200 MB

DT 12Z 28/6/82 VT 12Z 28/6/82 MAIN T+0 TEMPERATURE C. 200 MB

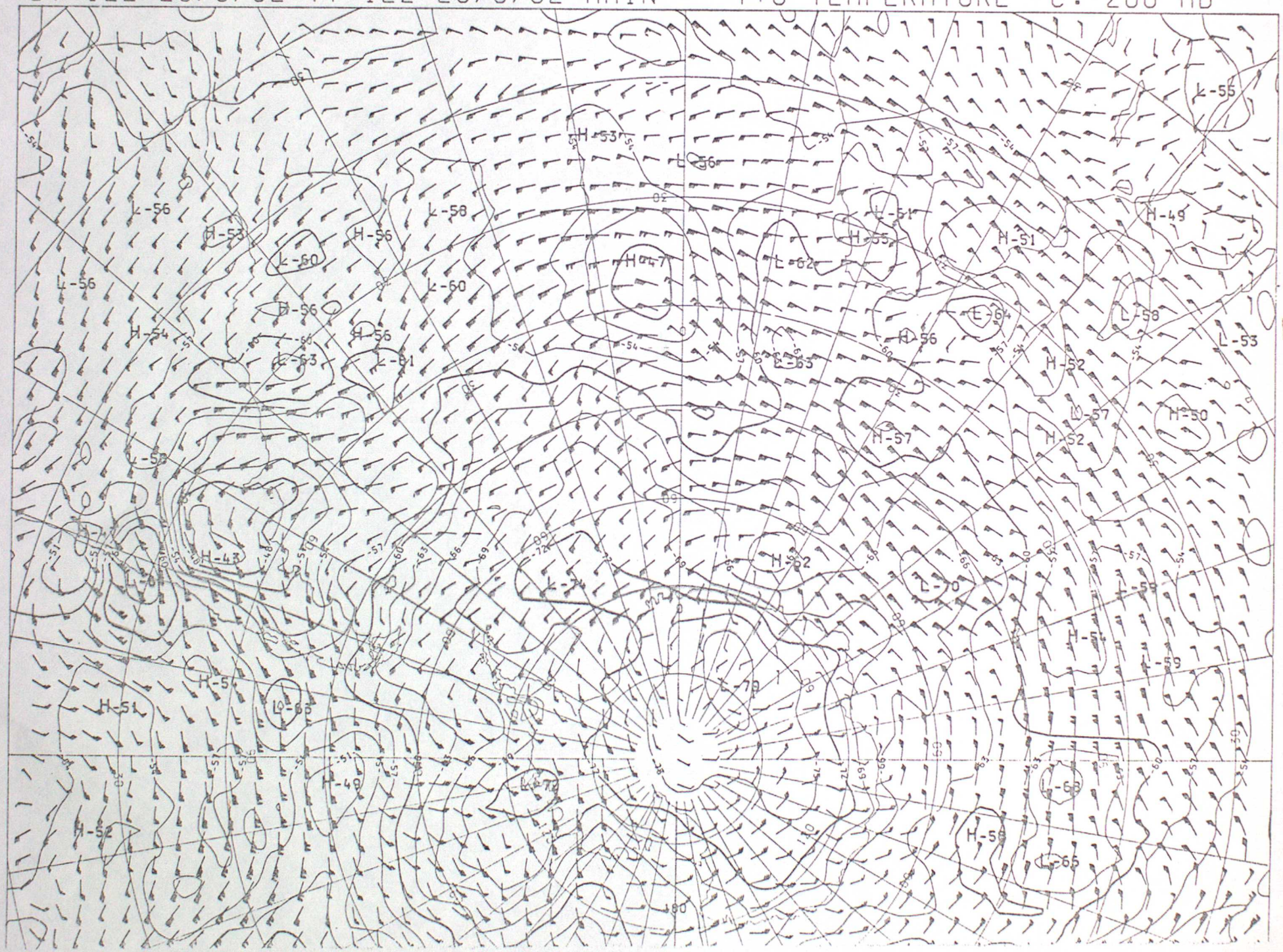

FIG 1(e)

DT 12Z 28/6/82 VT 12Z 28/6/82 MAIN T+0 DDFF KT. STR 150 MB

DT 12Z 28/6/82 VT 12Z 28/6/82 MAIN T+0 TEMPERATURE C. 150 MB

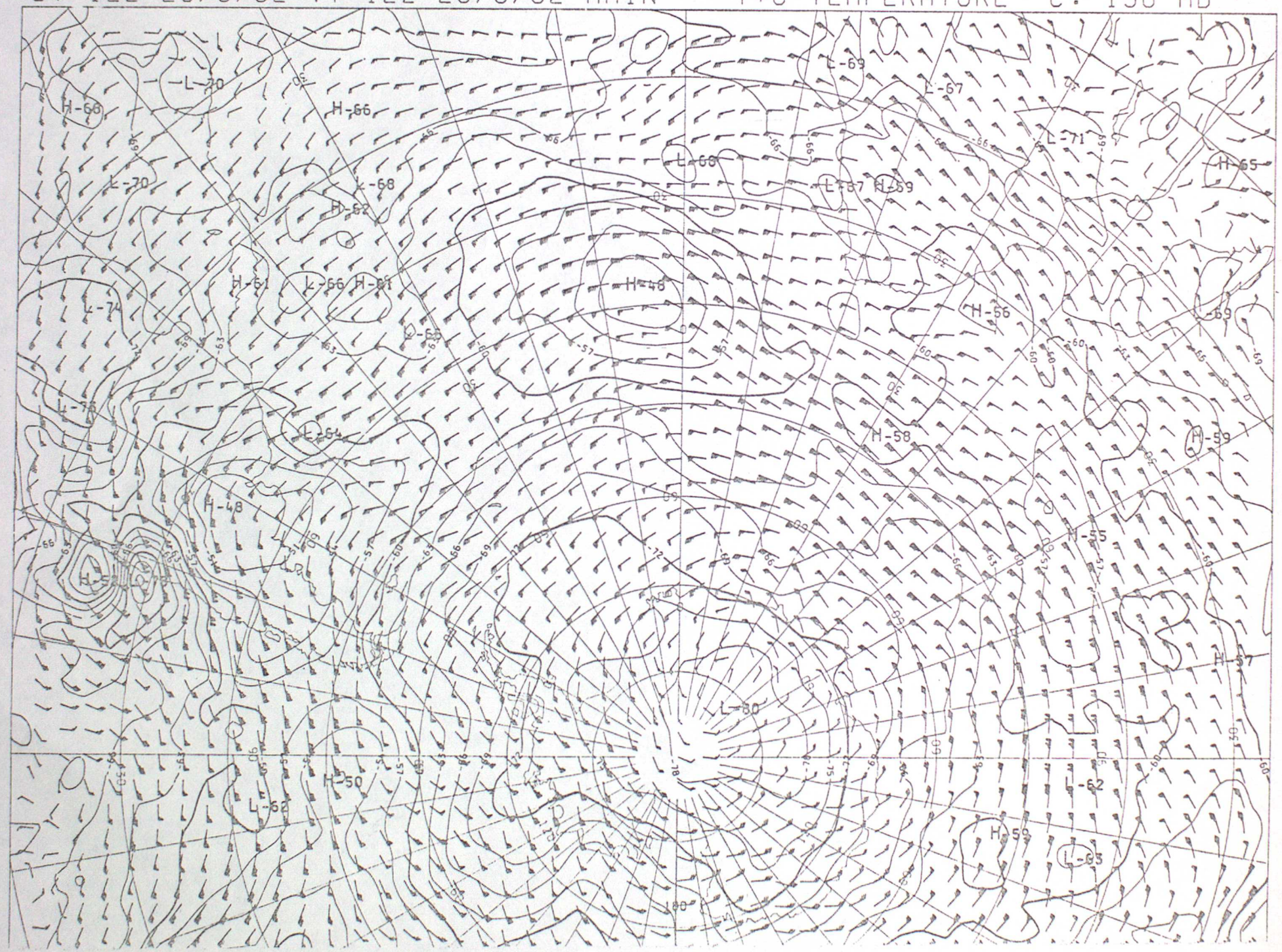

FIG 16)

COP

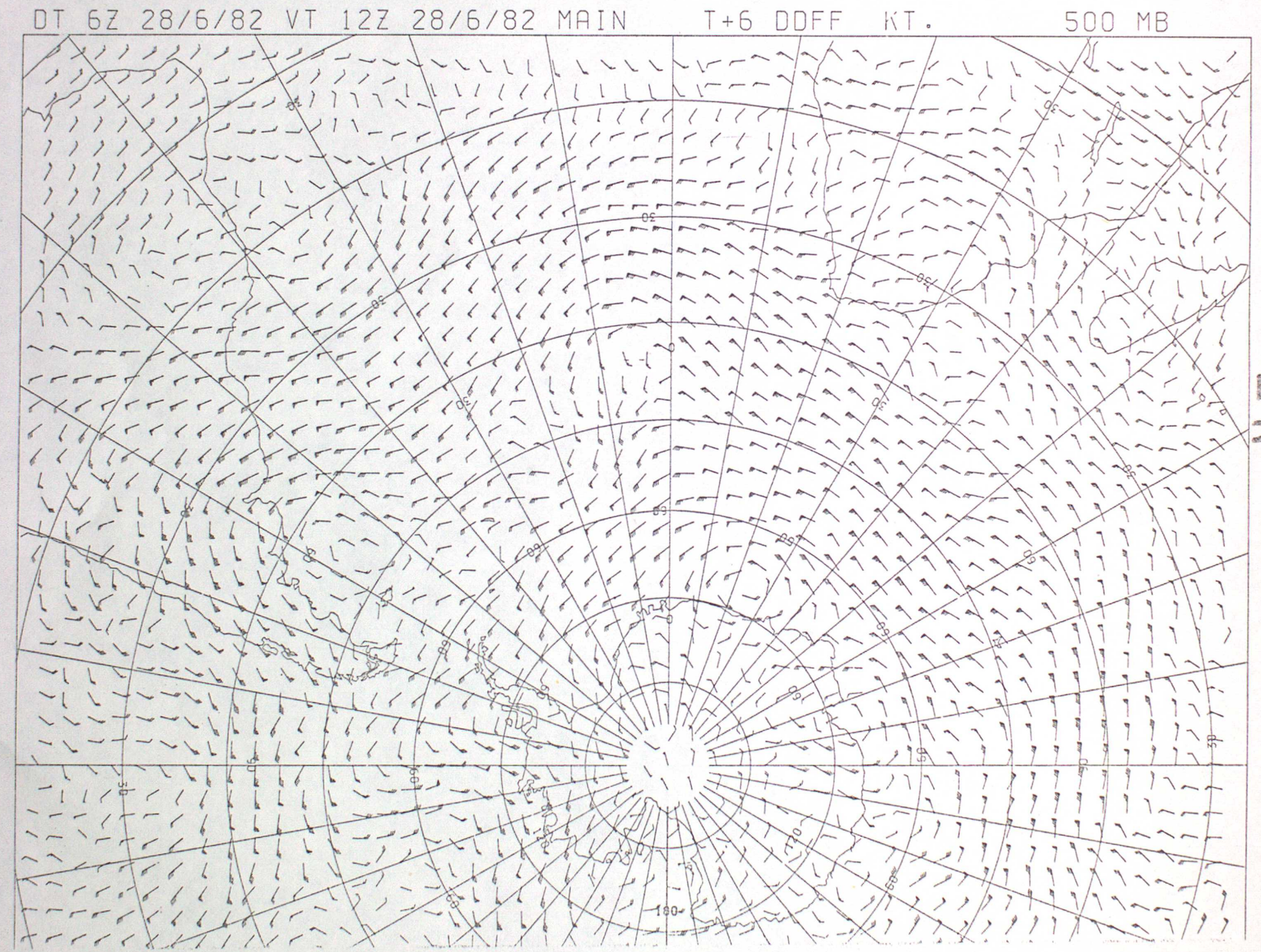

FIG 2(a)

COP

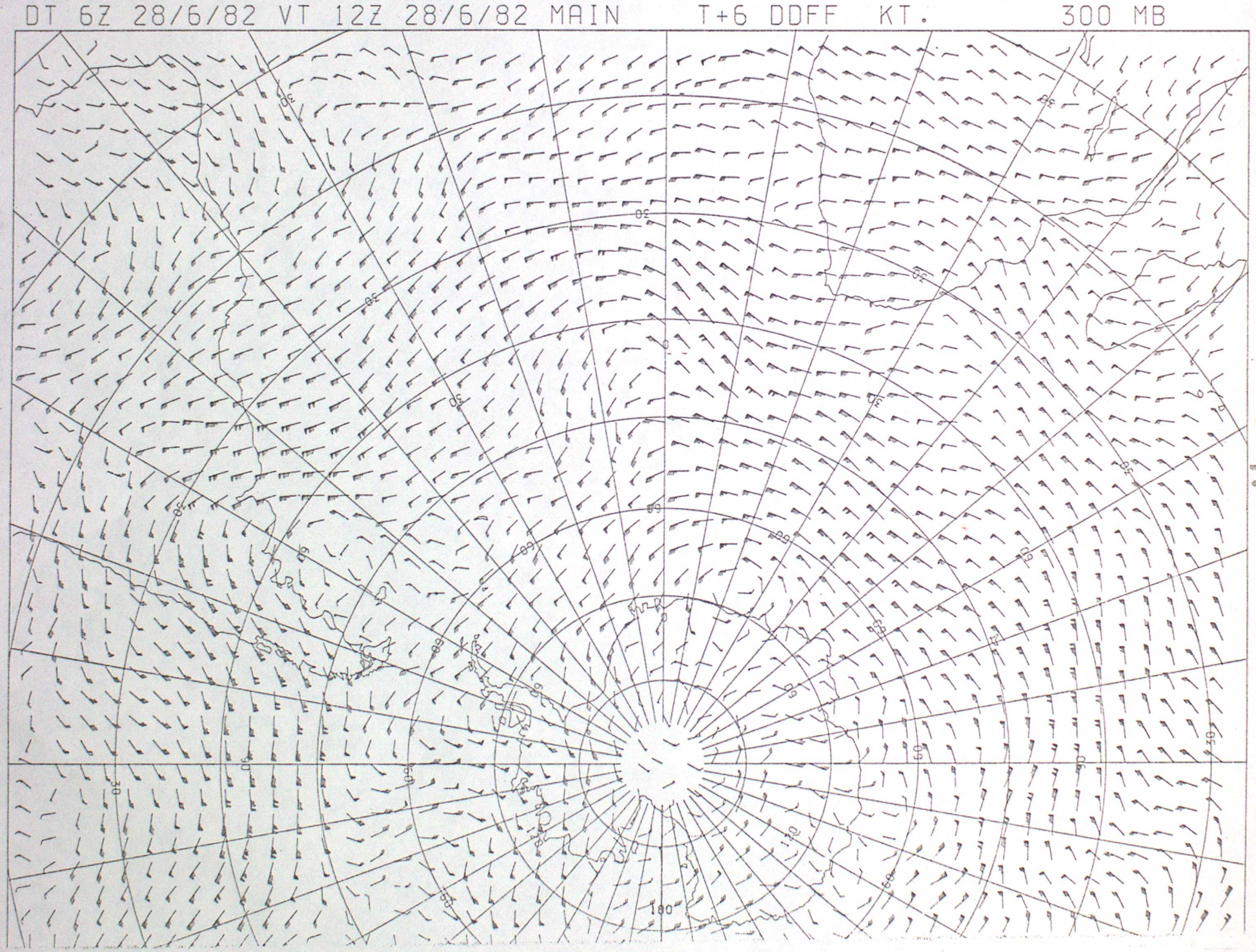
DT 6Z 28/6/82 VT 12Z 28/6/82 MAIN T+6 DDFF KT. 300 MB
30
60
90
120
150
180

FIG 2(b)

DT 12Z 28/6/82 VT 12Z 29/6/82 MAIN T+24 DDFF KT. STR 700 MB

DT 12Z 28/6/82 VT 12Z 29/6/82 MAIN T+24 TEMPERATURE C. 700 MB

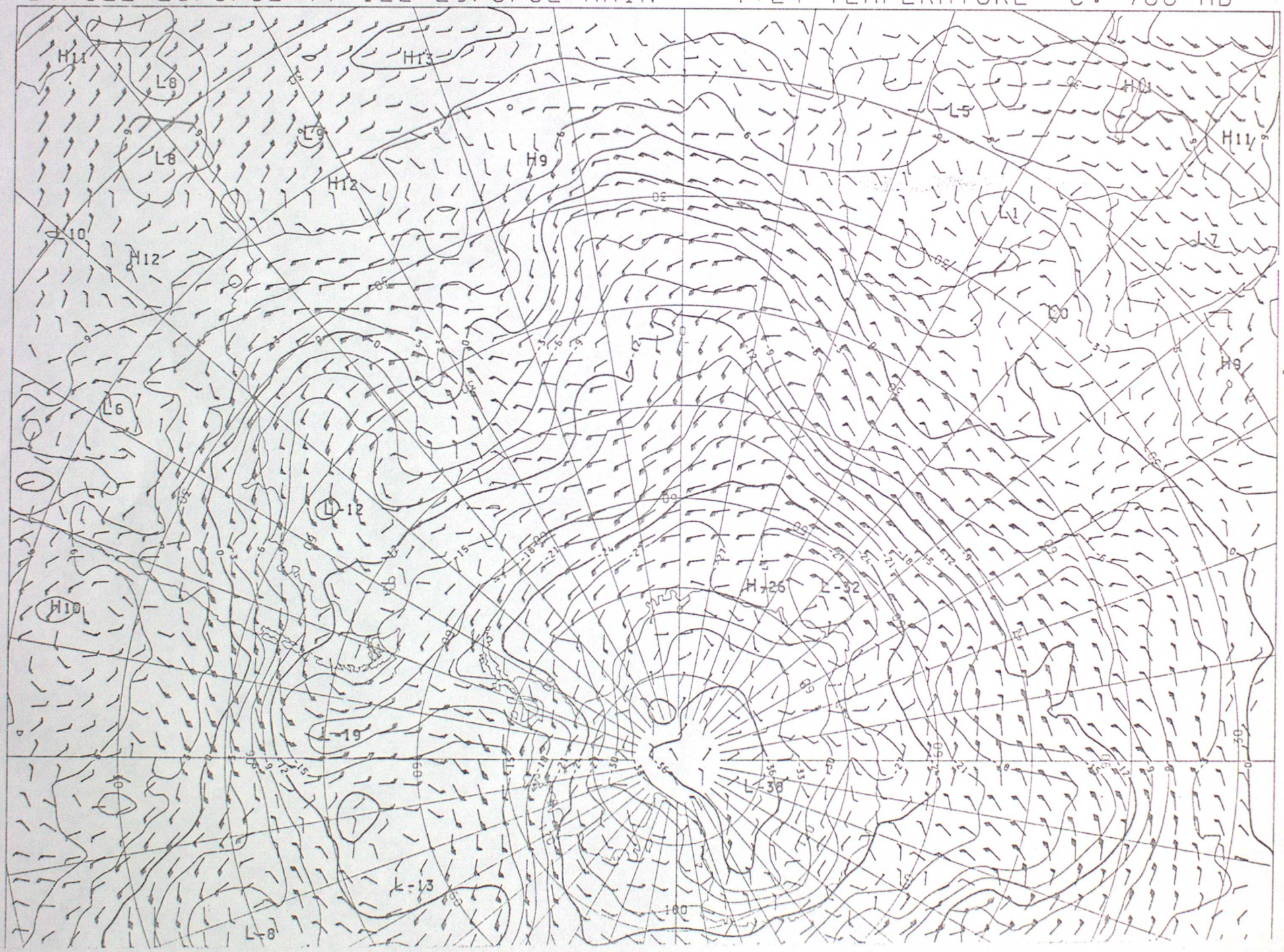

FIG 2(a)

DT 12Z 28/6/82 VT 12Z 29/6/82 MAIN T+24 DDFF KT. STR 300 MB

DT 12Z 28/6/82 VT 12Z 29/6/82 MAIN T+24 TEMPERATURE C. 300 MB

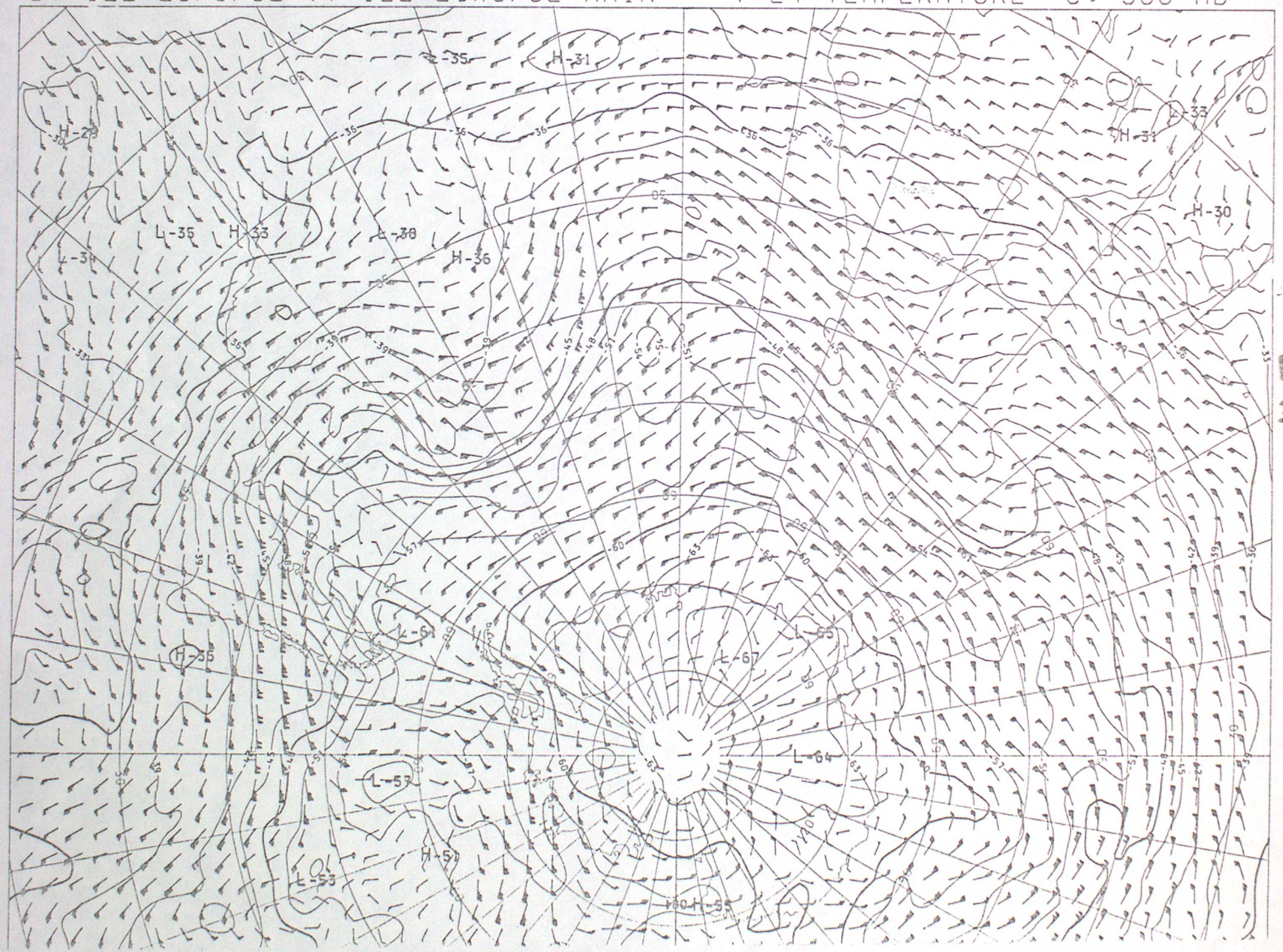

FIG 3(b)

FIGURE 4 (a) 12Z, 28/6/82

ROOT MEAN SQUARE PRESSURE TENDENCY FOR AREA 13·5°-28·5°S, 99·4°-52·5°W

$\overline{\left(\frac{\partial p_*}{\partial t}\right)^2}^{1/2}$ mb/hr

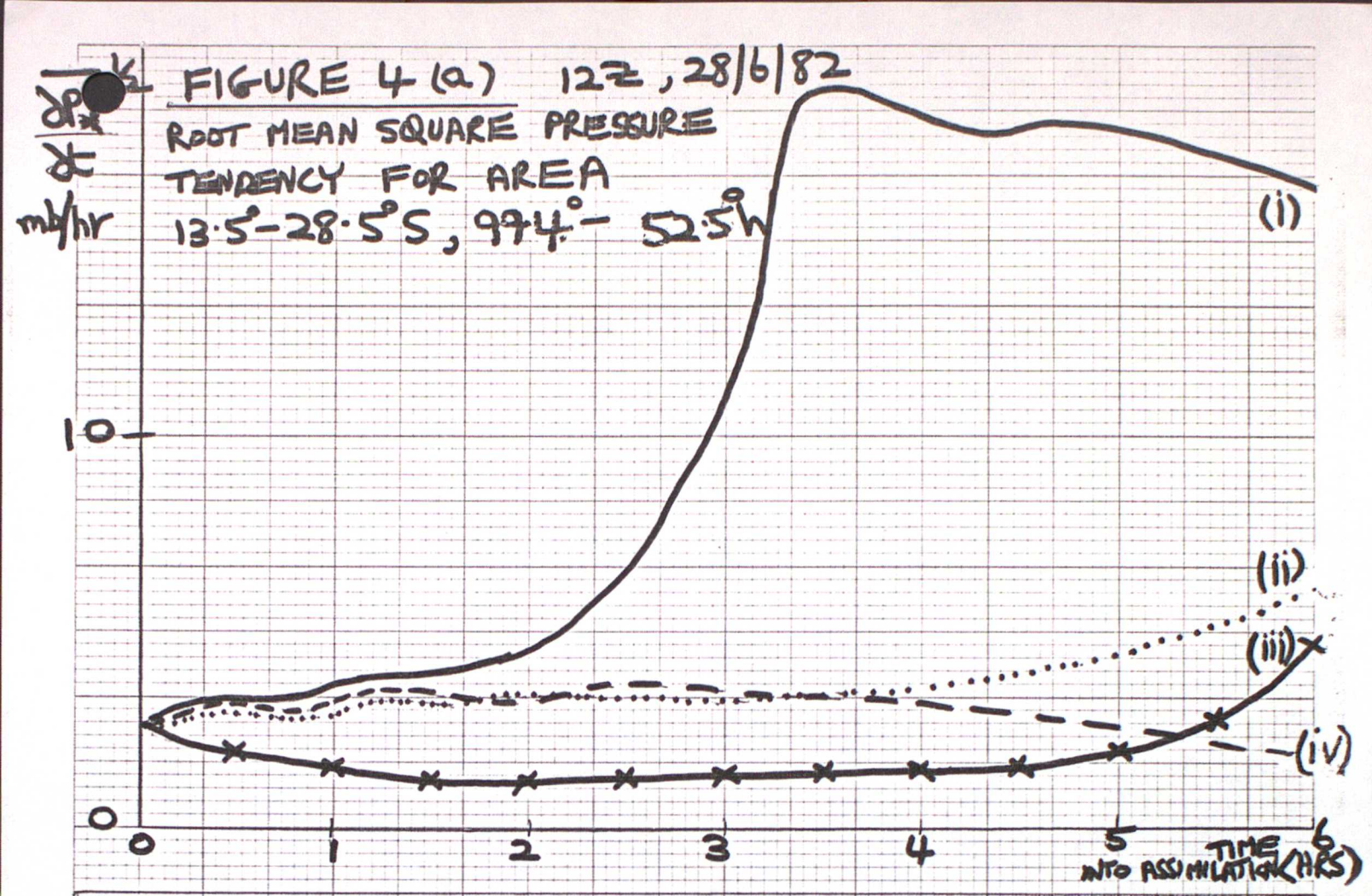

FIGURE 4 (b) 12Z, 28/6/82

ROOT MEAN SQUARE DIVERGENCE FOR AREA 13·5°-28·5°S, 99·4°-52·5°W σ LEVELS 1-15

$\overline{|\nabla \cdot V|^2}^{1/2}$ $\times 10^4 s^{-1}$

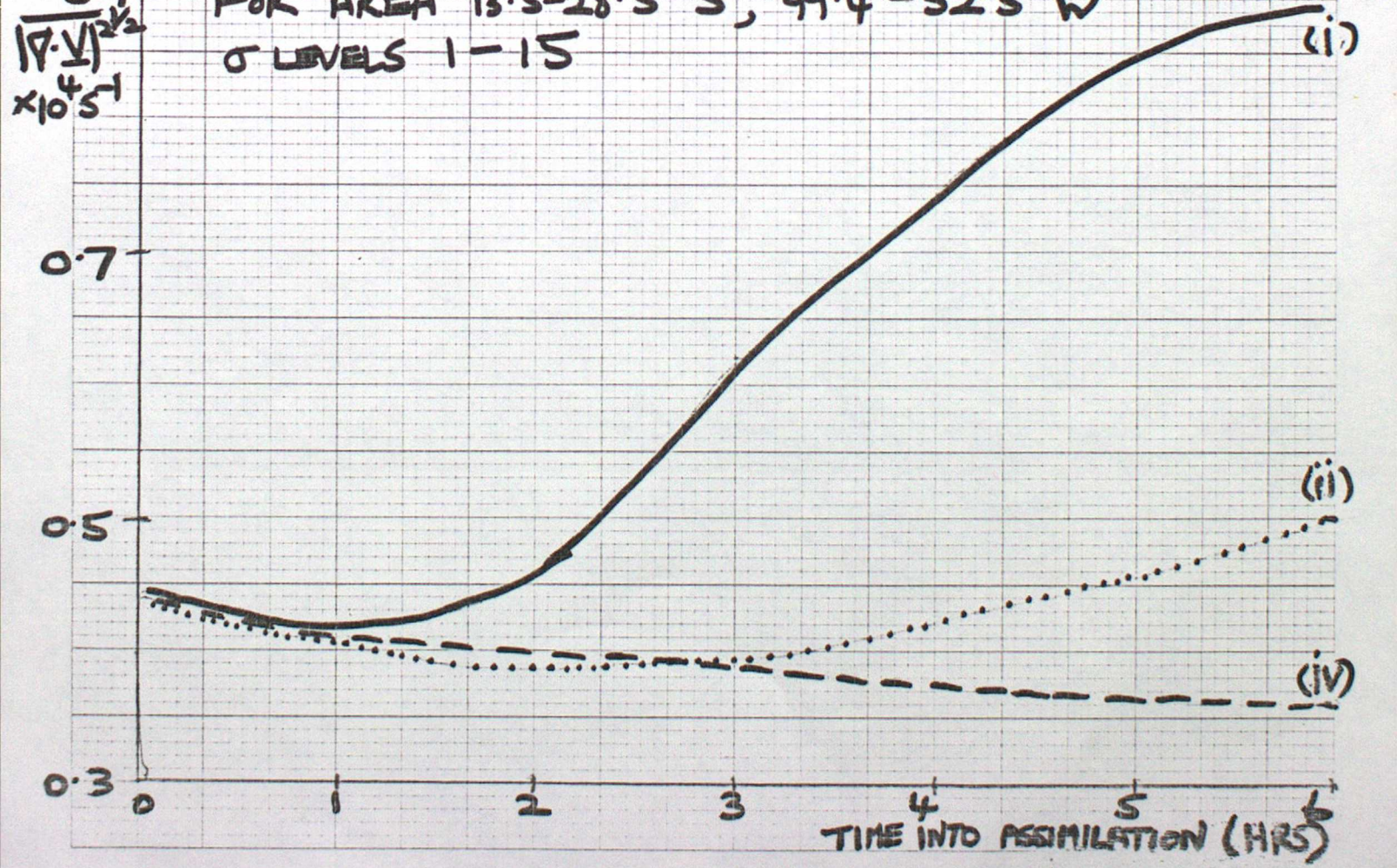

FIGURE 4(c) 122, 28/6/82

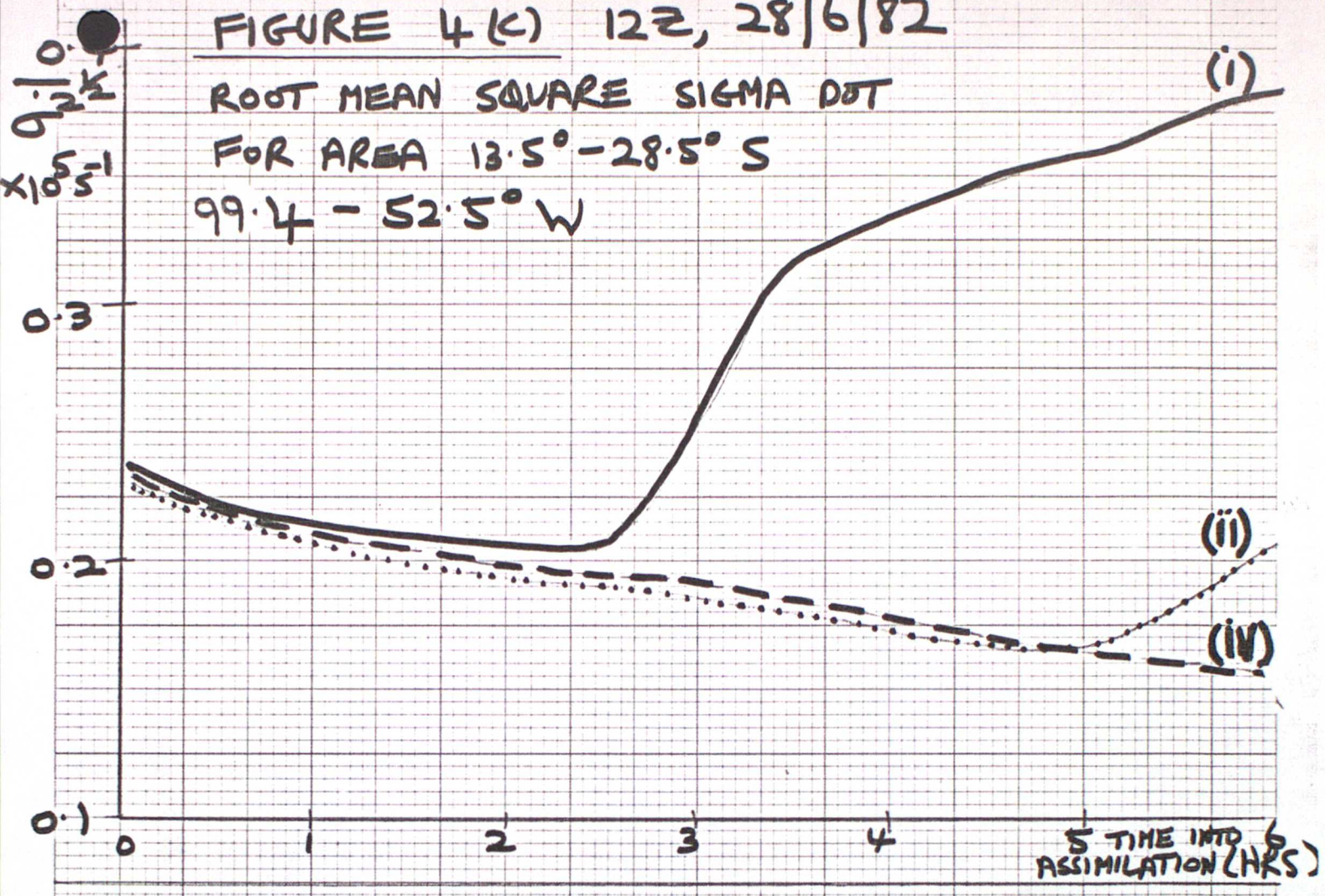

KEY TO FIGURES 4 AND 5

EXPERIMENT

(i) —— RELAXATION COEFFICIENT 0·1, DAMPING OF INTEGRATED DIVERGENCES, PRESSURE LEVEL ANALYSIS

(ii) ..... RELAXATION COEFFICIENT VARYING LINEARLY 0 → 0·1. DAMPING INTEGRATED DIVERGENCES PRESSURE LEVEL ANALYSIS

(iii) ×—× RELAXATION COEFFICIENT VARYING LINEARLY 0 → 0·125. DAMPING DIVERGENCES LEVEL BY LEVEL. PRESSURE LEVEL ANALYSIS (ONLY FG 4(a))

(iv) – – – RELAXATION COEFFICIENT 0·1, DAMPING OF INTEGRATED DIVERGENCES. SIGMA LEVEL ANALYSIS

FIGURE 5(a) EXPERIMENT (i) · $\sigma = 0.69$

ROWS 75-78

POINTS 152-155

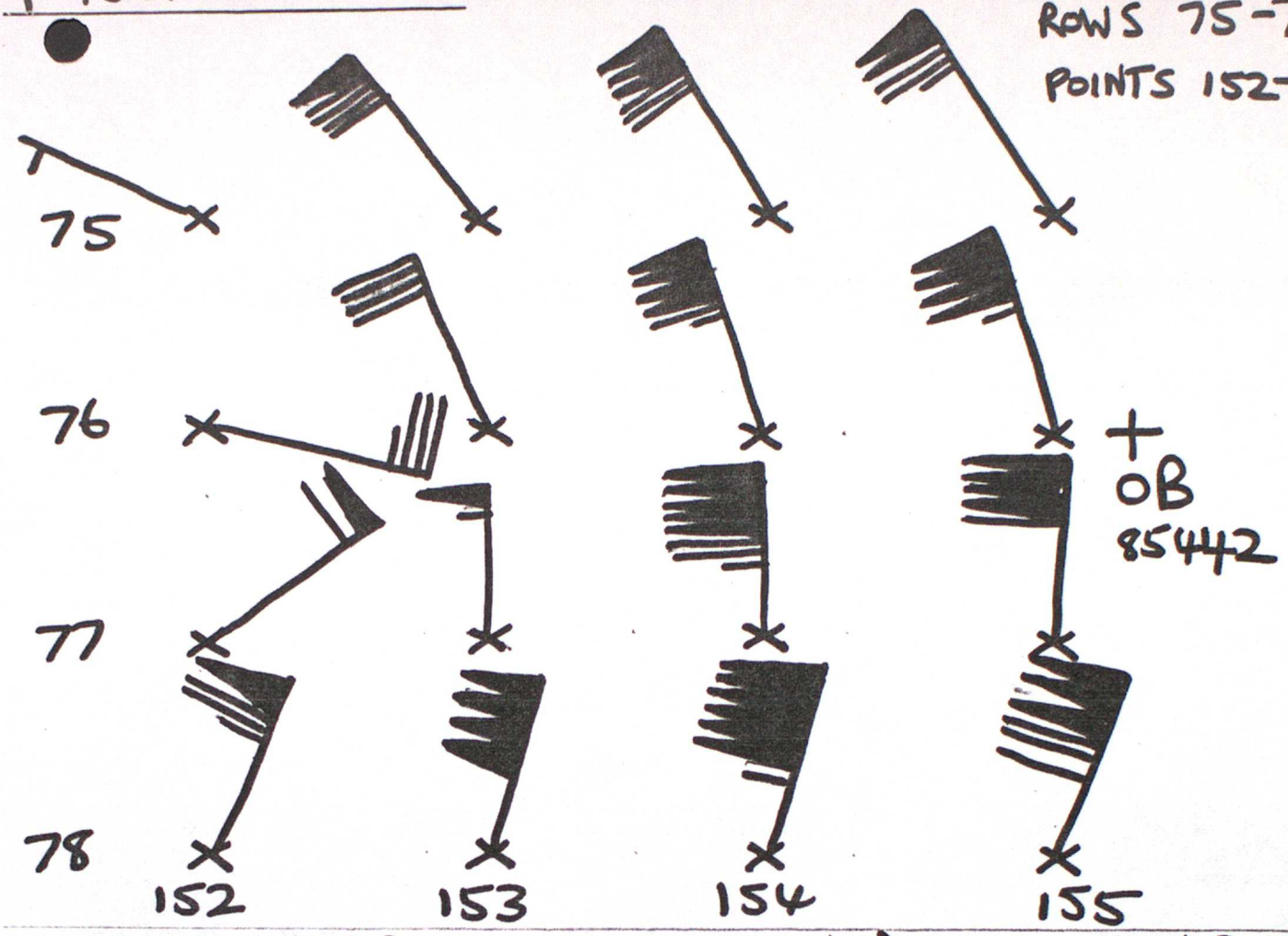

FIGURE 5(b) EXPERIMENT (ii) $\sigma = 0.69$

ROWS 75-78

POINTS 152-155

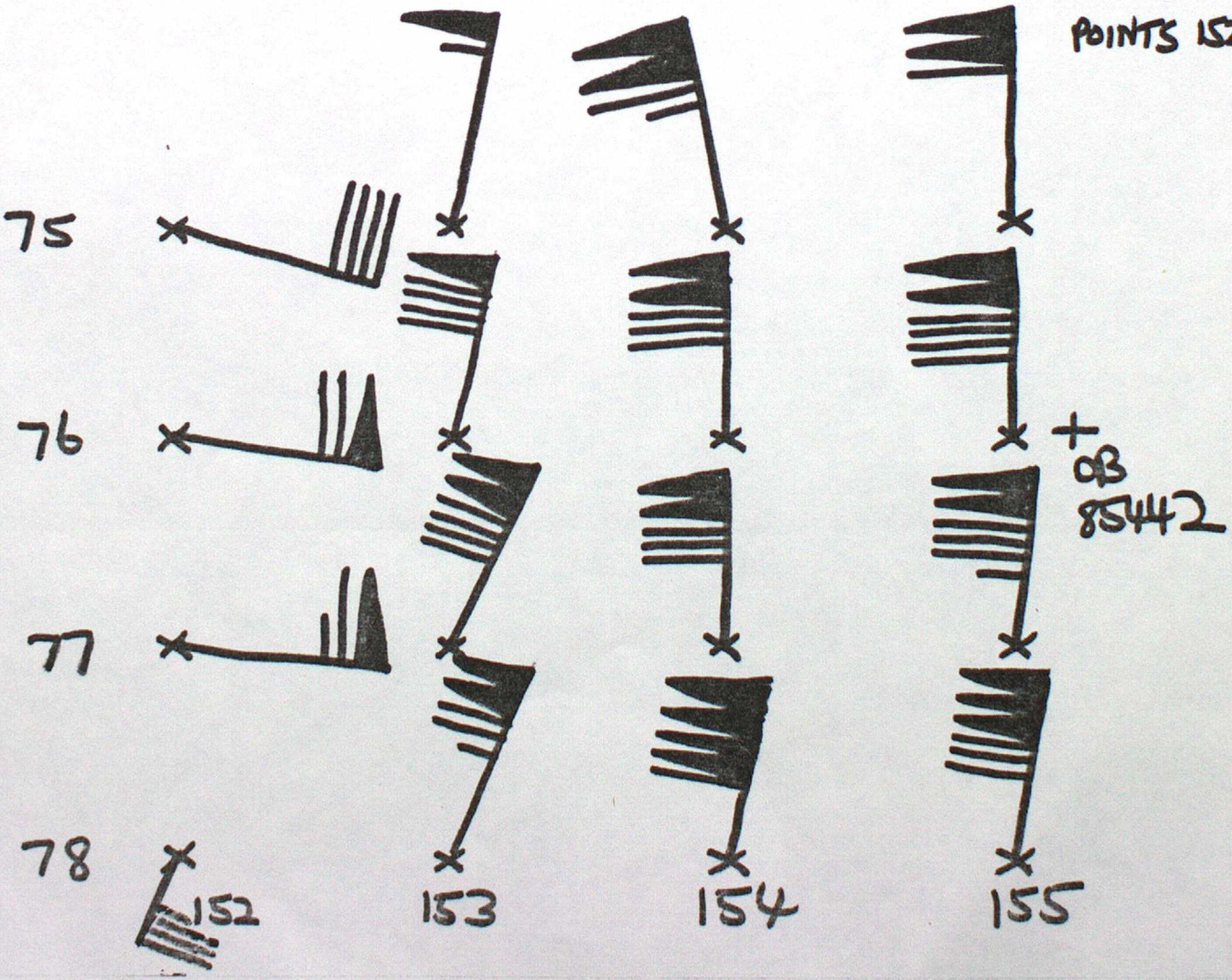

FIGURE 5(c) EXPERIMENT (iii) $\sigma = 0.69$

ROWS 75-78
POINTS 152-155

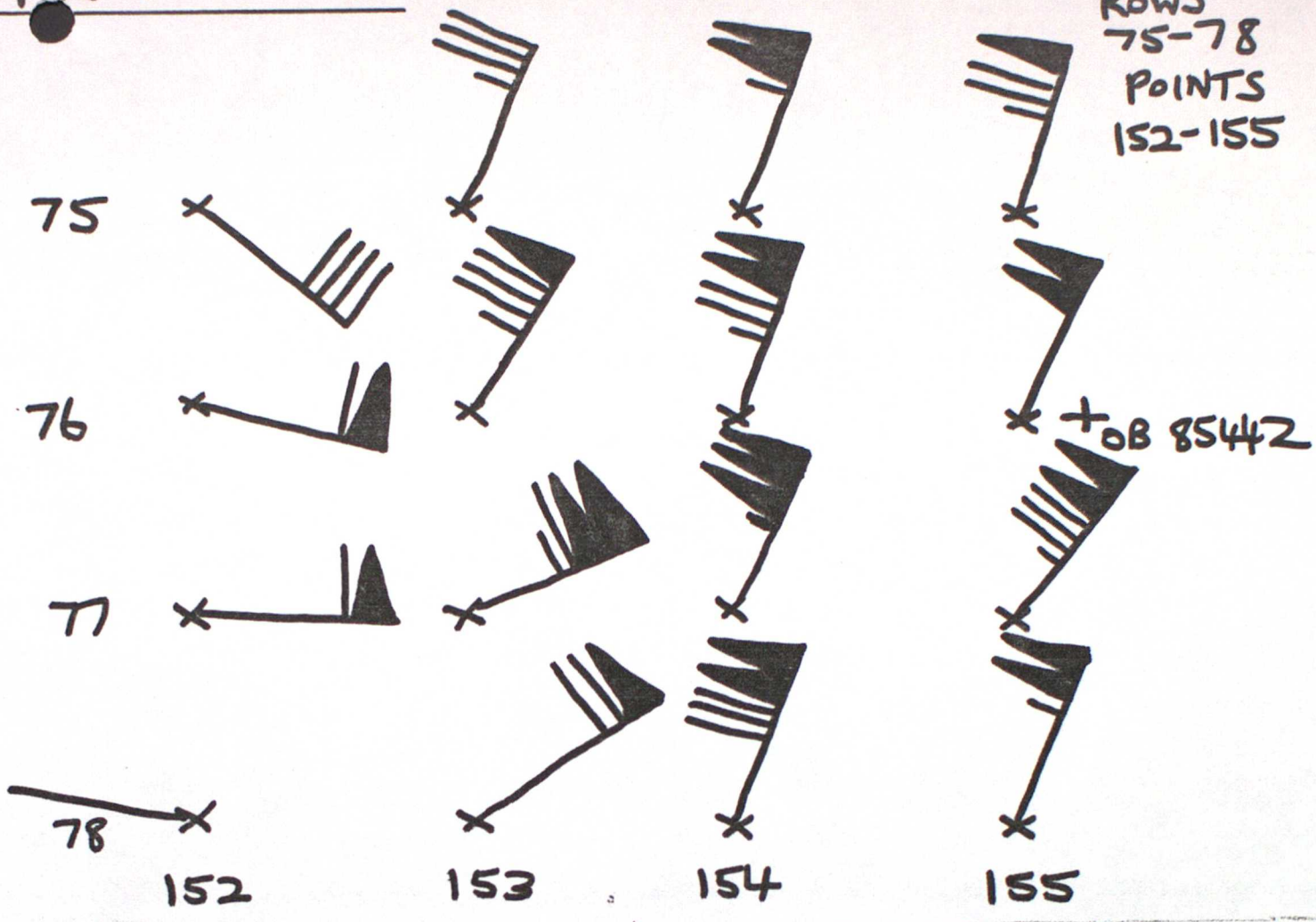

FIGURE 5(d) EXPERIMENT (iv) $\sigma = 0.69$

ROWS 75-78
POINTS 152-155

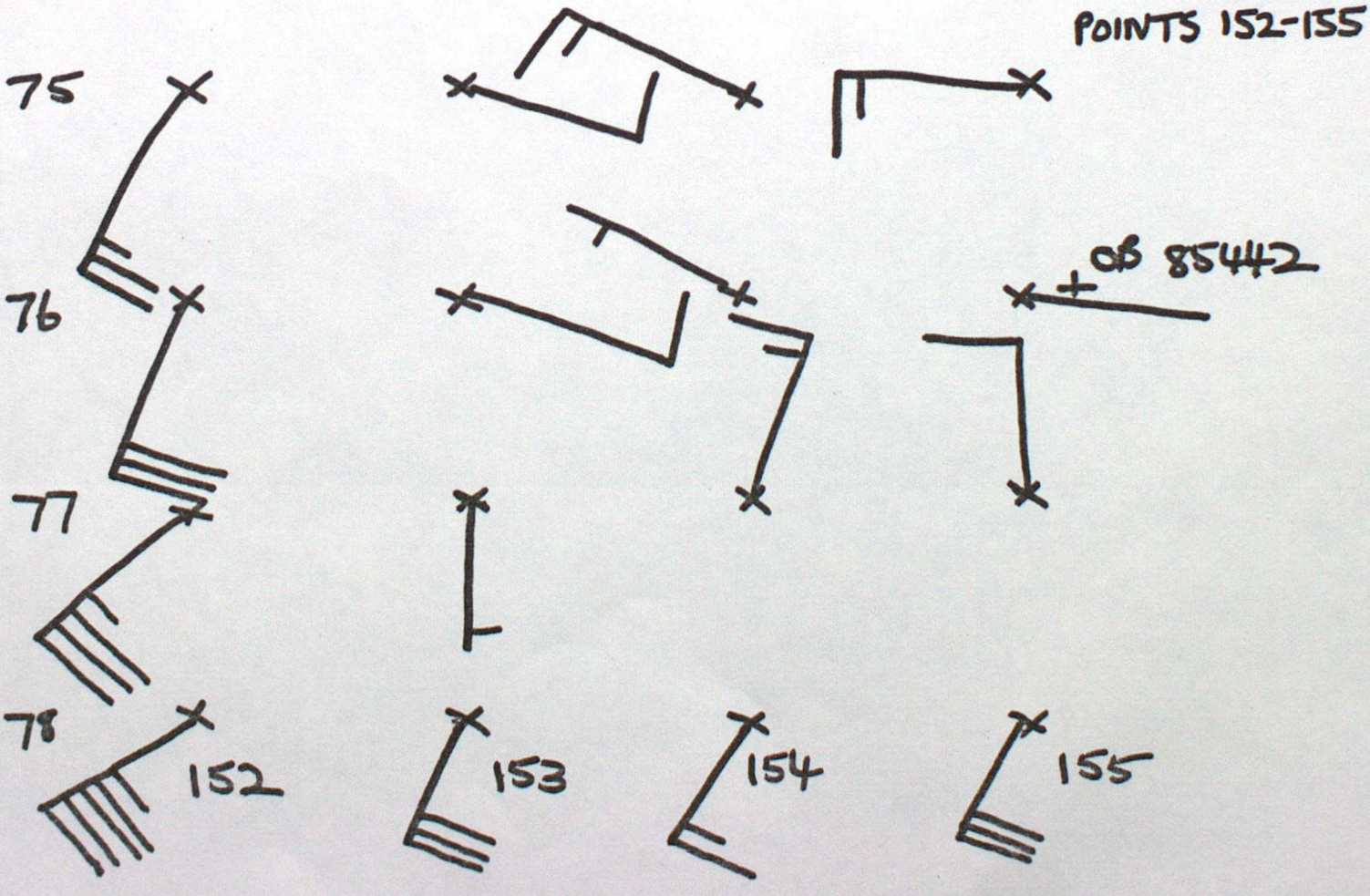

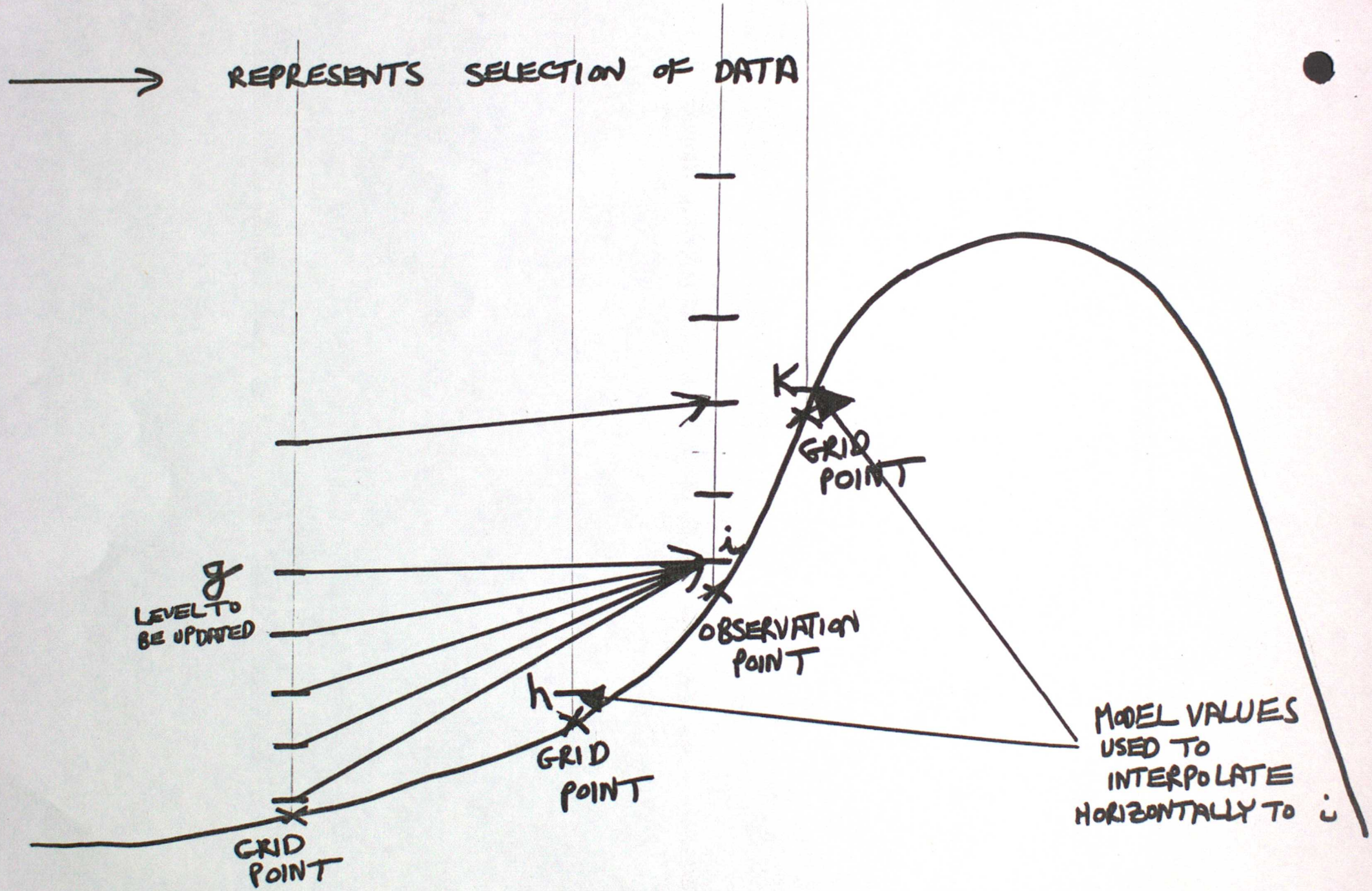

FIGURE 6 SCHEMATIC DIAGRAM OF DATA SELECTION ACCORDING TO PRESSURE LEVEL

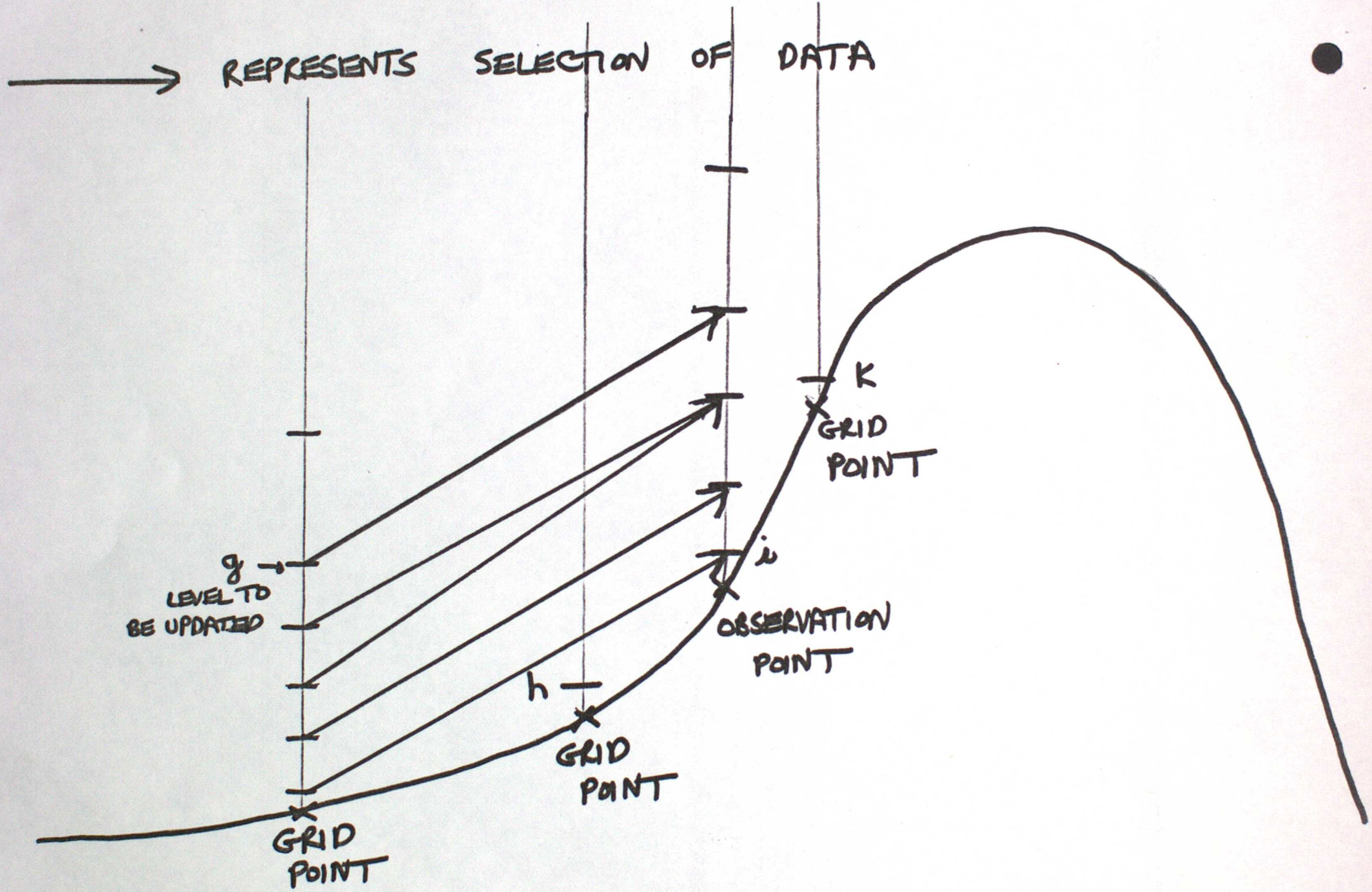

FIGURE 7 SCHEMATIC DIAGRAM OF DATA SELECTION ACCORDING TO SIGMA LEVEL

DT 12Z MON 28/6/82 VT 12Z MON 28/6/82 MAIN T+0 DDFF KT. 700 MB

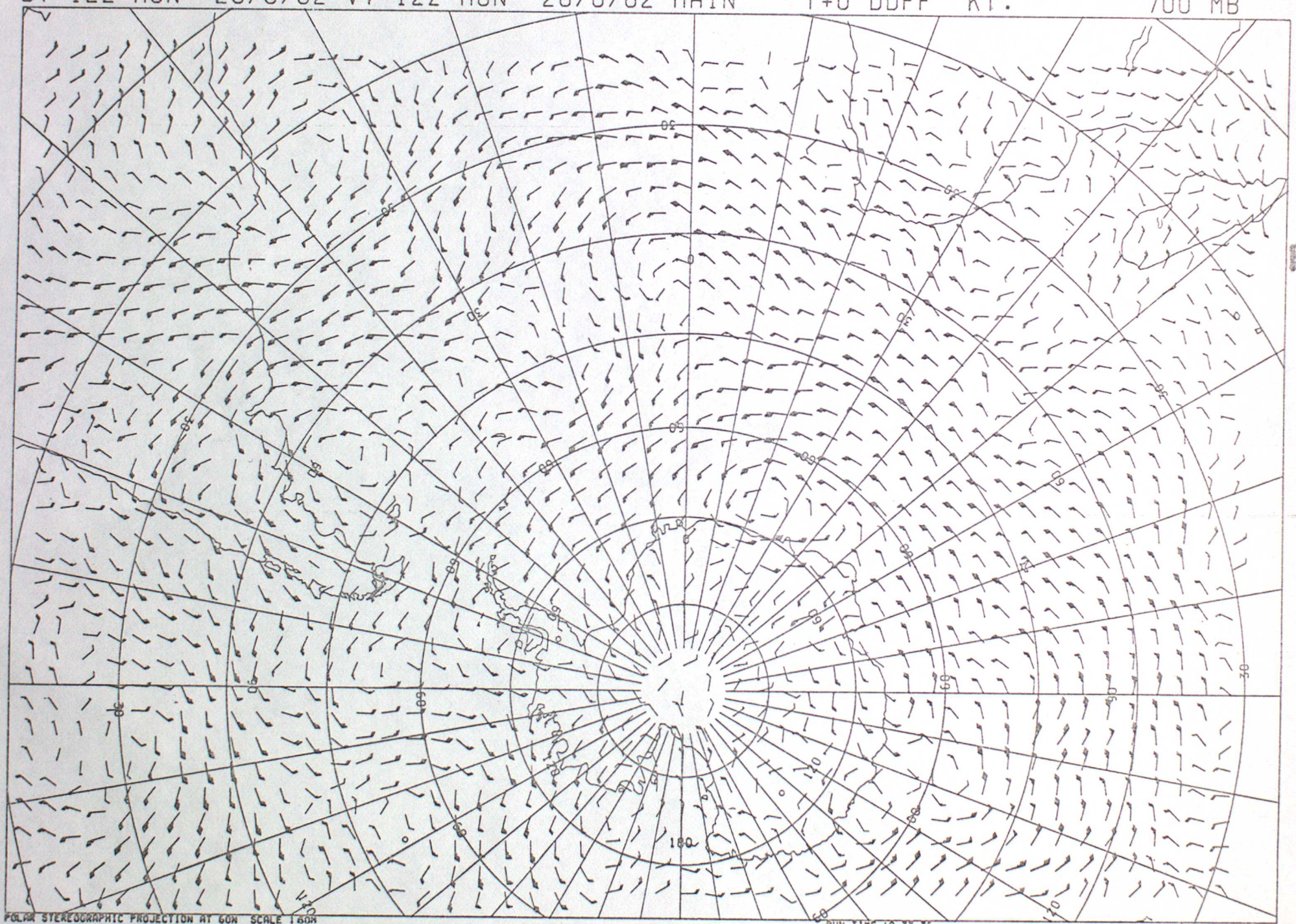

FIG 8(a)

POLAR STEREOGRAPHIC PROJECTION AT 60N SCALE 1:60M

RUN TIME 10.33.36

COP

CHART 425

DT 12Z MON 28/6/82 VT 12Z MON 28/6/82 MAIN T+0 DDFF KT. 500 MB

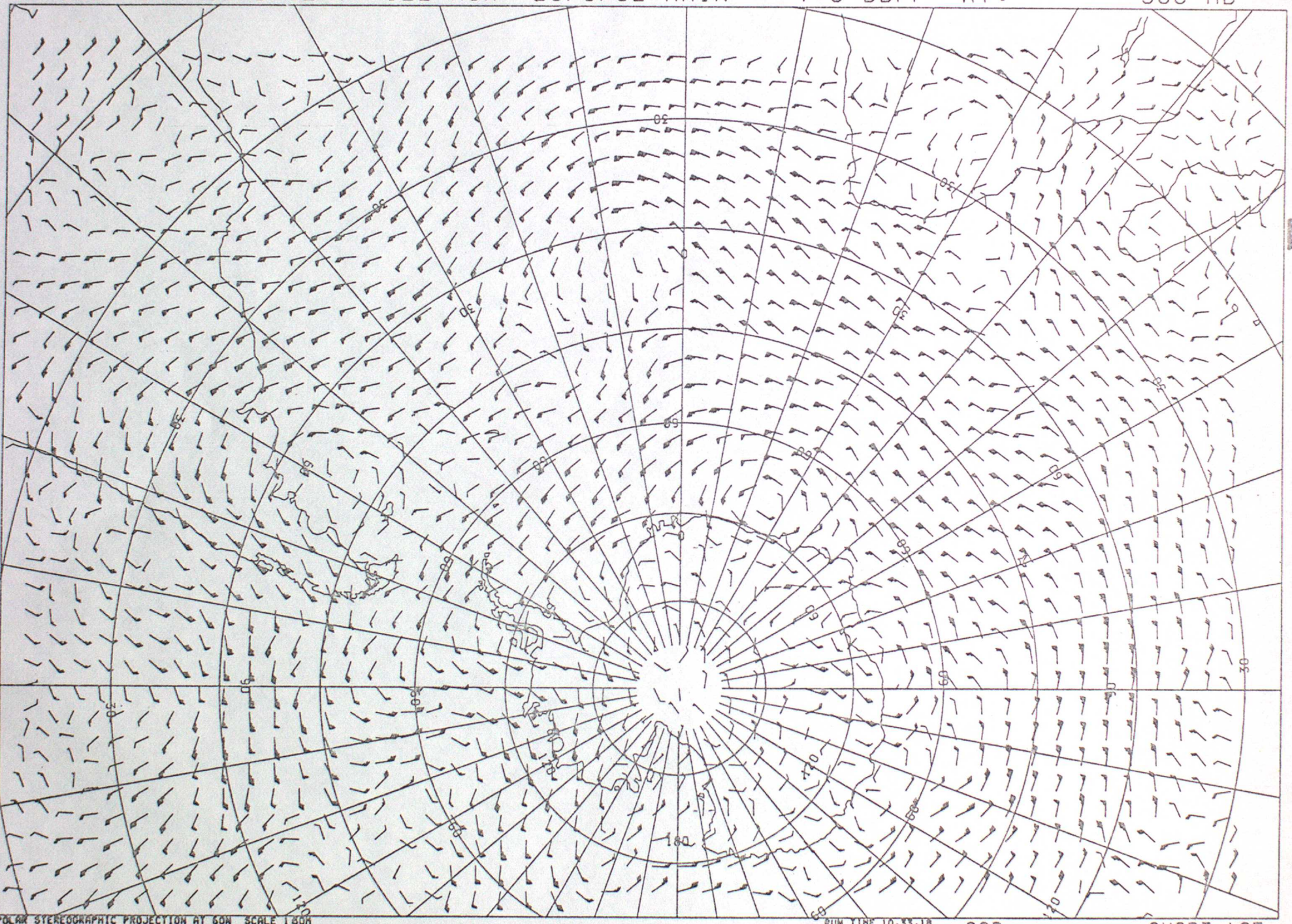

FIG 8(b)

POLAR STEREOGRAPHIC PROJECTION AT 60N SCALE 1:80M

RUN TIME 10.33.18

COP

CHART 425

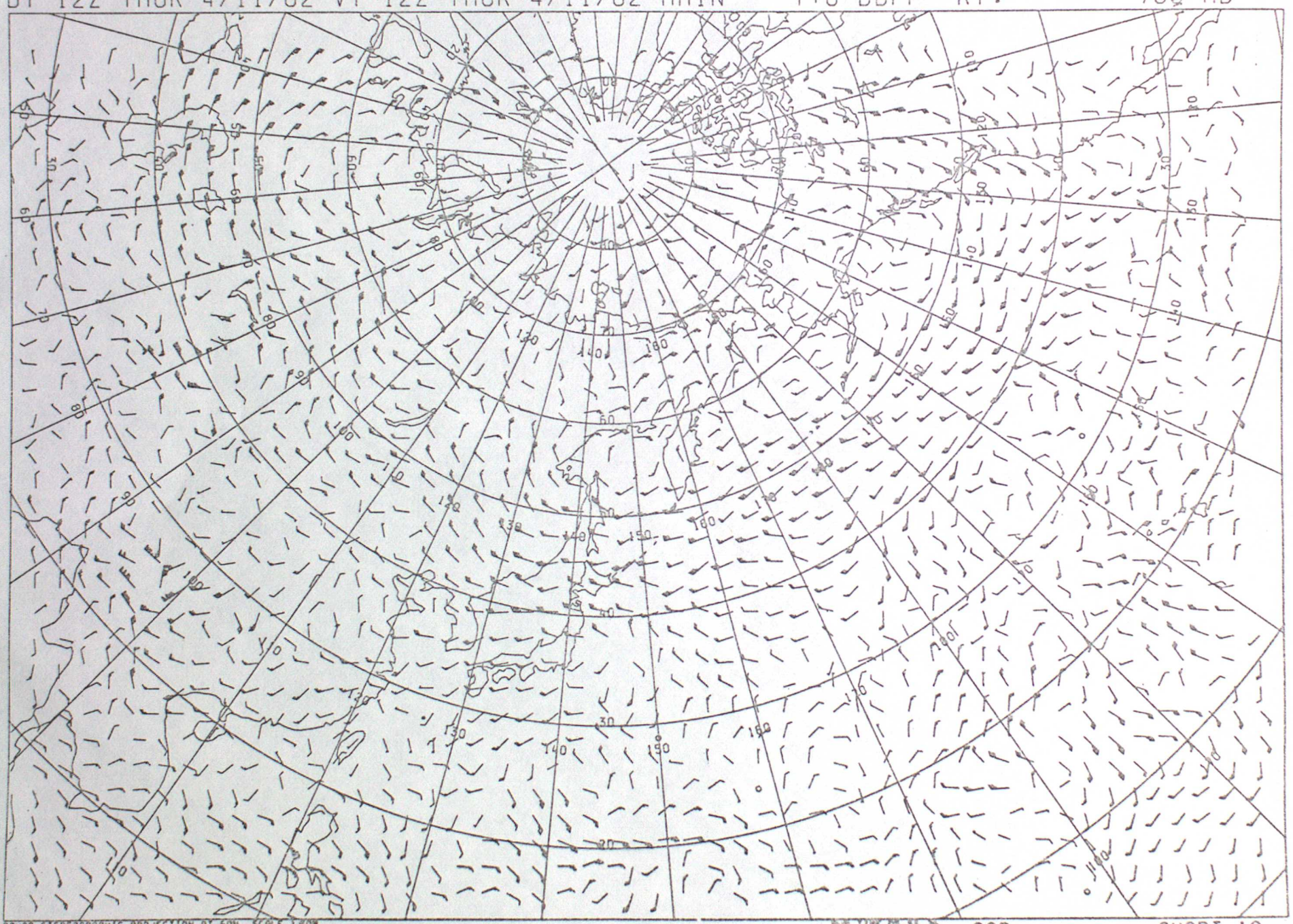

FIG 9 (a)

PRESSURE LEVEL ANALYSIS

RELAXATION COEFFICIENT = 0.3

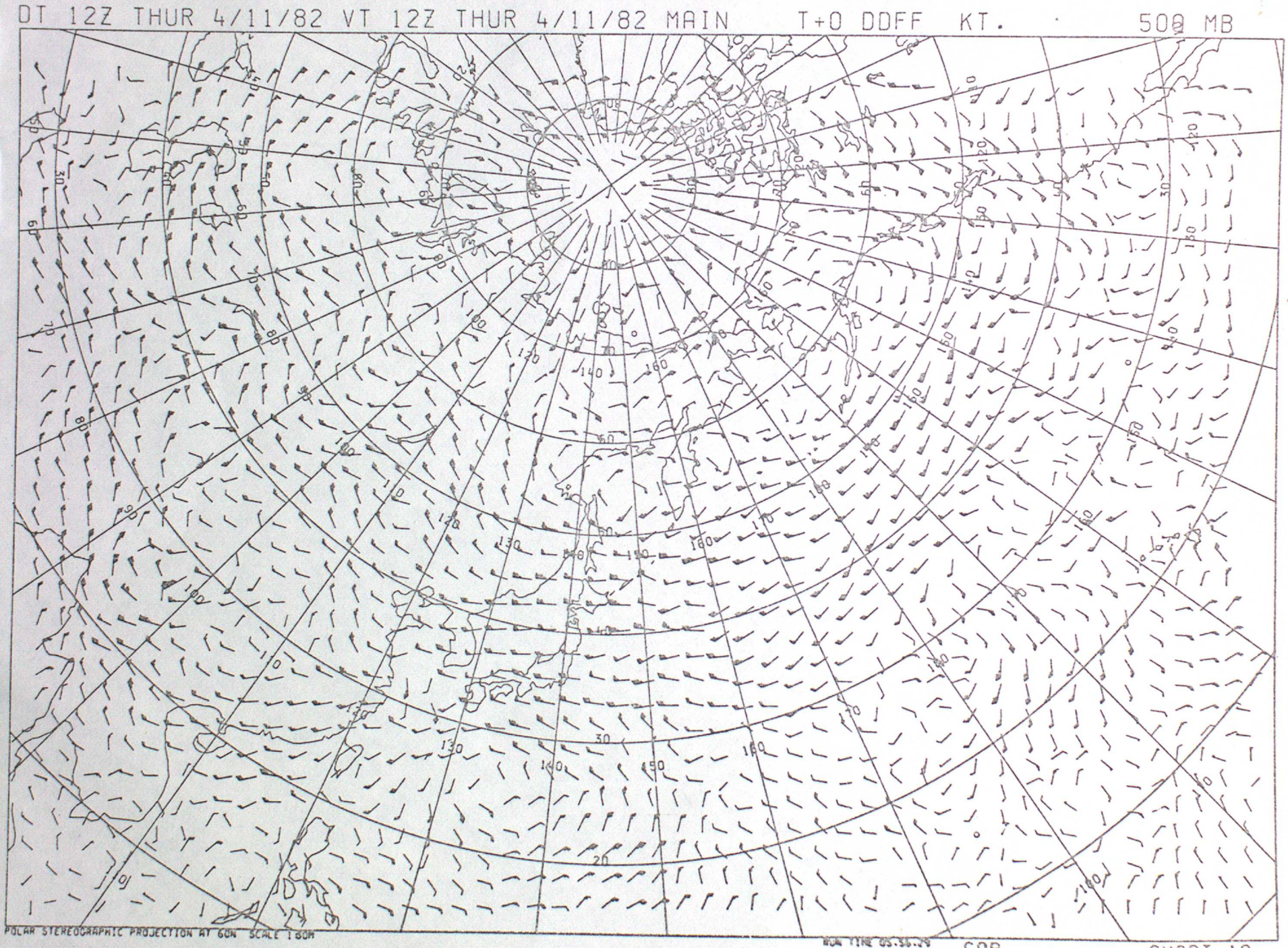

FIG-9(b)

PRESSURE LEVEL ANALYSIS

RELAXATION COEFFICIENT = 0·3

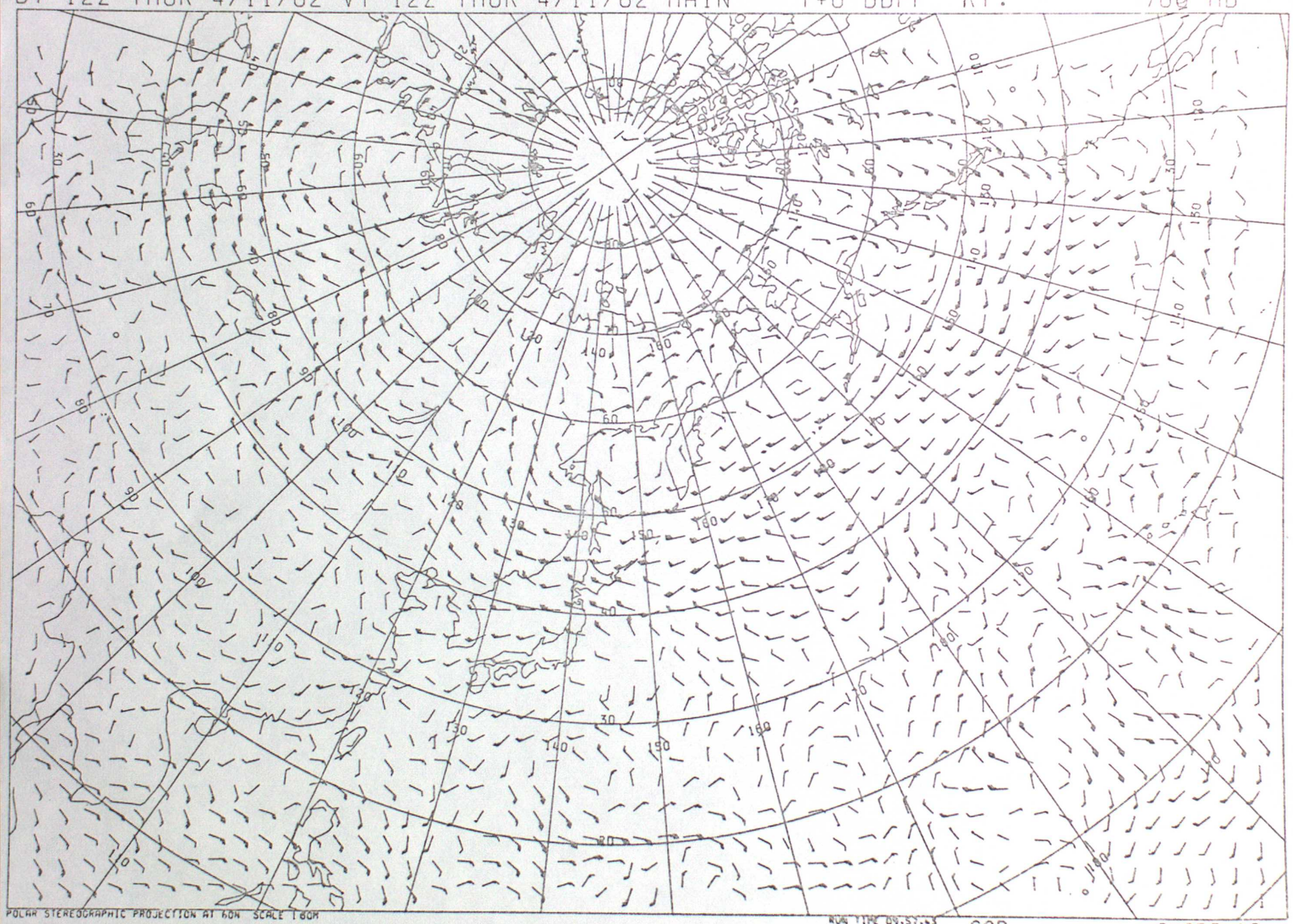

FIGURE 10(a)

SIGMA LEVEL ANALYSIS RELAXATION COEFFICIENT = 0.3

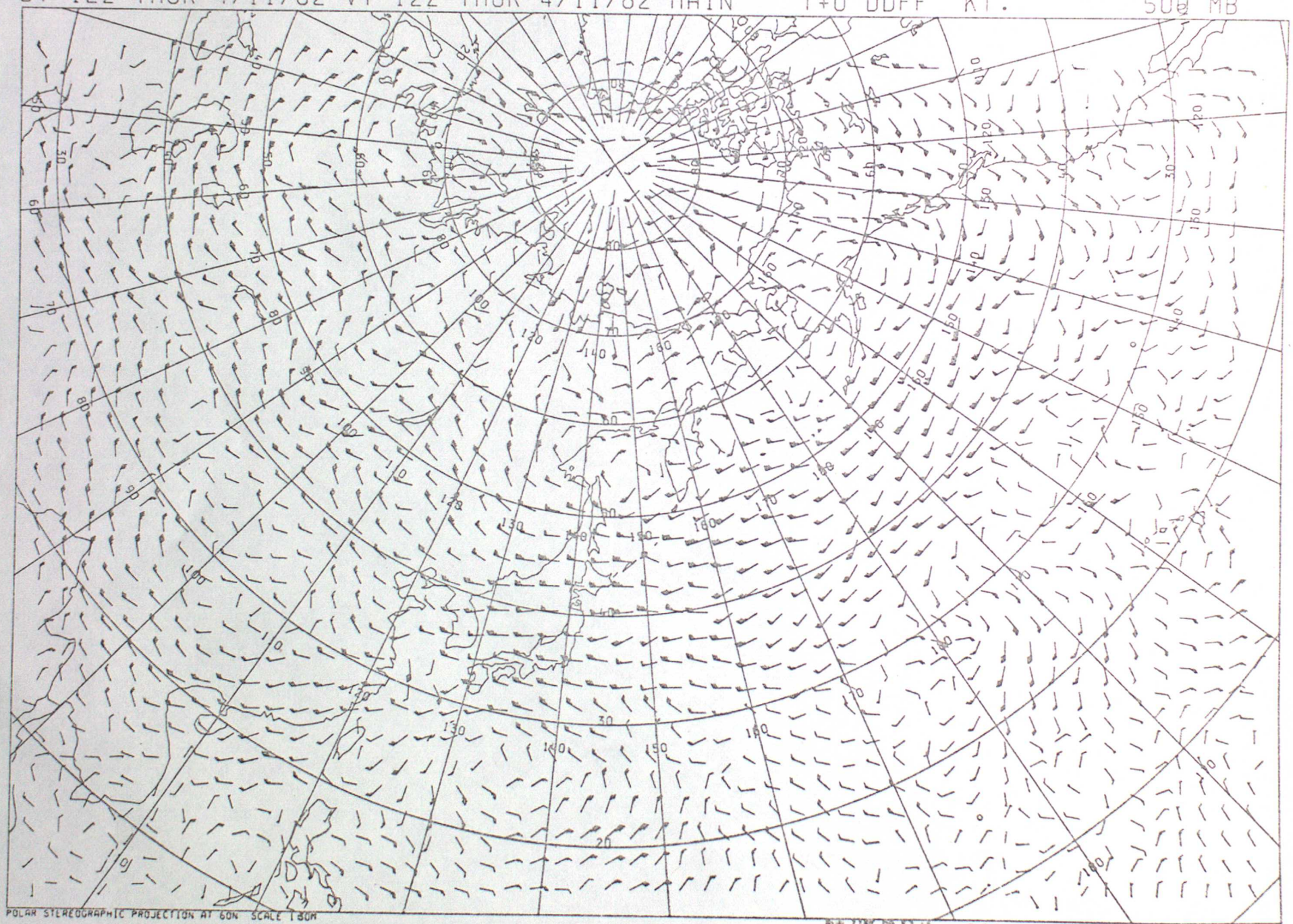

FIGURE 10(b)

SIGMA LEVEL ANALYSIS

RELAXATION COEFFICIENT = 0·3